

Oblique projection for scalable rank-adaptive reduced-order modeling of nonlinear stochastic PDEs with time-dependent bases

M. Donello¹, G. Palkar¹, M.H. Naderi¹, D. C. Del Rey Fernández², and Hessam Babae^{*1}

¹Department of Mechanical Engineering and Materials Science, University of Pittsburgh

²Department of Applied Mathematics, University of Waterloo

Abstract

Time-dependent basis reduced order models (TDB ROMs) have successfully been used for approximating the solution to nonlinear stochastic partial differential equations (PDEs). For many practical problems of interest, discretizing these PDEs results in massive matrix differential equations (MDEs) that are too expensive to solve using conventional methods. While TDB ROMs have the potential to significantly reduce this computational burden, they still suffer from the following challenges: (i) inefficient for general nonlinearities, (ii) intrusive implementation, (iii) ill-conditioned in the presence of small singular values, and (iv) error accumulation due to fixed rank. To this end, we present a scalable method based on oblique projections for solving TDB ROMs that is computationally efficient, minimally intrusive, robust in the presence of small singular values, rank-adaptive, and highly parallelizable. These favorable properties are achieved via low-rank approximation of the time discrete MDE. Using the discrete empirical interpolation method (DEIM), a low-rank decomposition is computed at each iteration of the time stepping scheme, enabling a near-optimal approximation at a fraction of the cost. We coin the new approach TDB-CUR since it is equivalent to a CUR decomposition based on sparse row and column samples of the MDE. We also propose a rank-adaptive procedure to control the error on-the-fly. Numerical results demonstrate the accuracy, efficiency, and robustness of the new method for a diverse set of problems.

1 Introduction

Discretizations of many time-dependent partial differential equations (PDEs) result in matrix differential equations (MDEs) in the form of $d\mathbf{V}/dt = \mathcal{F}(\mathbf{V})$, where $\mathbf{V} \in \mathbb{R}^{n \times s}$ is the solution matrix and $\mathcal{F}(\mathbf{V}) \in \mathbb{R}^{n \times s}$ is obtained by discretizing the PDE in all dimensions except time. One such example is the uncertainty propagation of random parameters into the PDEs, which requires solving the PDEs for a large number of random realizations [31, 48]. Discretization of this problem can be formulated as an MDE, where the rows of the matrix are obtained by discretizing the PDE in the physical domain and the columns of the matrix are samples of the discretized equation for a particular choice of random parameters.

*Corresponding author. Email:h.babae@pitt.edu.

For high-dimensional PDEs subject to high-dimensional random parameters, the resulting MDEs can be massive. For example, uncertainty quantification of a 3D time-dependent fluid flow typically requires solving an MDE with $n \sim \mathcal{O}(10^6) - \mathcal{O}(10^9)$ grid points (rows) and $s \sim \mathcal{O}(10^4) - \mathcal{O}(10^7)$ random samples (columns). Therefore, the solution to these massive MDEs is cost prohibitive due to the floating point operations (flops), memory, and storage requirements. The discretization of many other PDEs can also be cast as MDEs, for example, kinetics equations [24, 28, 33], linear sensitivity analyses [22] and species transport equations in turbulent combustion [45].

For many practical applications, $\mathbf{V}(t)$ is instantaneously low-rank. Therefore, low-rank approximations using time-dependent bases (TDBs) have the potential to significantly reduce the computational cost of solving massive MDEs. For these systems, a TDB-based low-rank approximation extracts low-rank structures via TDBs for the column and row spaces of \mathbf{V} . A reduced-order model (ROM) is then constructed by projecting the full-order model (FOM) onto the column and row TDBs. Low-rank approximation based on TDB was first introduced in the quantum chemistry field to solve the Schrödinger equation [9], and it is commonly known as the multiconfiguration time-dependent Hartree (MCTDH) method. The MCTDH methodology was later presented for generic MDEs in [31] and is referred to as dynamical low-rank approximation (DLRA).

Various TDB ROM schemes have also been developed to solve stochastic partial differential equations (SPDEs). Dynamically orthogonal (DO) decomposition [48], bi-orthogonal (BO) decomposition [18], dual dynamically orthogonal (DDO) decomposition [37], and dynamically bi-orthogonal decomposition (DBO) [40] are all TDB-based low-rank approximation techniques for solving stochastic PDEs (SPDEs). In all of these decompositions (DO, BO, DDO, and DBO), an evolution equation for the mean field is developed, along with evolution equations for the TDB-ROM of the mean-subtracted stochastic fields. Although these decompositions have different forms and constraints, they are all equivalent, i.e., they produce identical low-rank matrices [19, 40], and their differences lie only in their numerical performance. TDB ROMs have also been used in other fields and applications including dynamical systems [21, 42], combustion [39, 45], linear sensitivity analysis [22], dynamical instabilities [4, 10, 11], deep learning [49], and singular value decomposition (SVD) estimation for matrices that vary smoothly with a parameter [53].

Despite the potential of using TDB ROMs to significantly reduce the computational cost of solving massive MDEs, there are still a number of outstanding challenges for most practical problems of interest. We summarize three key challenges below:

- (i) **Computational efficiency:** For specific classes of equations (e.g. homogeneous linear and quadratic nonlinear), rank- r TDB ROMs can be solved efficiently with operations that scale with $\mathcal{O}(nr)$ and $\mathcal{O}(sr)$ for linear MDEs or scale with $\mathcal{O}(nr^2)$ and $\mathcal{O}(sr^2)$ for quadratic MDEs. However, this computational efficiency is lost for general nonlinearities, requiring operations that scale with the size of the FOM, i.e., $\mathcal{O}(ns)$.
- (ii) **Intrusiveness:** Even in the special cases of homogeneous linear and quadratic nonlinear equations, efficient implementation of TDB ROM evolution equations is an intrusive process [38, Appendix B]. This involves replacing the low-rank approximation in the FOM, projecting the resulting equation onto the tangent manifold, and obtaining low-rank matrices for each term on the right-hand side. The process requires significant effort to derive, implement, and debug the code. This poses a major

obstacle for most practitioners, creating a significant barrier to adopting the methodology.

- (iii) **Ill-conditioning:** The TDB ROM evolution equations become numerically unstable when the singular values of the low-rank approximation become very small. This is particularly problematic because it is often necessary to retain very small singular values in order to have an accurate approximation. Small singular values lead to ill-conditioned matrices that require inversion in all variations of TDB ROM evolution equations [18, 31, 37, 40, 48], resulting in restrictive time step limitations for numerical integration and error amplification.

Although some of these challenges have been tackled, there is currently no methodology that can address all of them. In particular, the problems of ill-conditioning and computational expense must be resolved for practitioners to adopt TDB-based low-rank approximations for MDEs. To address the issue of ill-conditioning, a projector-splitting time integration was proposed [34], in which arbitrarily small singular values can be retained. However, this scheme includes a backward time integration substep, which is an unstable substep for dissipative problems. To address this issue, an unconventional robust integrator was recently proposed [13] which retains the robustness with respect to small singular values while avoiding the unstable backward step. The authors also presented an elegant rank adaptive strategy, where the rank of the approximation changes over time to maintain a desired level of accuracy. Despite these advantages, this scheme is first-order in time [13, Theorem 4]. In [6], a pseudo-inverse methodology was presented as a remedy to maintain a well-conditioned system. However, in this approach, it is difficult to determine what singular value threshold must be used. Another projection method was presented in [30] that retains robustness with respect to small singular values and can be extended to high-order explicit time discretizations.

The three time-integration schemes presented in [13, 30, 34] and the pseudo-inverse methodology presented in [6] can retain $\mathcal{O}(n + s)$ cost for linear and quadratic MDEs. But achieving this speedup comes at the expense of a highly intrusive implementation. However, for generic nonlinear MDEs, an intrusive implementation is not possible, and the computational cost of solving the TDB ROMs using methods presented in [6, 13, 30, 34] scales with $\mathcal{O}(ns)$, which is the same as the cost of solving the FOM. Recently, a sparse interpolation algorithm was presented for solving the TDB ROM evolution equations with a computational complexity that scales with $\mathcal{O}(n + s)$ for generic nonlinear SPDEs [38]. However, this methodology still lacks robustness when the singular values become small, as it requires the inversion of the matrix of singular values.

In this work, we present a methodology inspired by interpolation and hyper-reduction techniques developed to accelerate nonlinear ROMs and finite-element models in vector differential equations [1, 7, 16, 25, 43, 47]. In particular, we present CUR factorizations of low-rank matrices that address the above challenges, i.e., (i) the computational cost of the methodology scales with $\mathcal{O}(n + s)$ for generic nonlinear SPDEs both in terms of flops and memory costs, (ii) it lends itself to simple implementation in existing codes, and (iii) the time-integration is robust in the presence of small singular values, and high-order explicit time integration can be used. To this end, the main elements of the presented methodology are (i) a time-discrete variational principle for minimization of the residual due to low-rank approximation error, and (ii) a CUR factorization based on strategic row and column sampling of the time discrete MDE.

The remainder of the paper is organized as follows: In Section 2, we first review the time continuous variational principle and its associated challenges. We then present the time discrete variational principle along with the rank-adaptive sparse sampling strategy for solving TDB-ROMs. Finally, we show that the resulting low-rank approximation is equivalent to a CUR factorization and we provide an upper bound on the approximation error. In Section 3, we demonstrate the method for a toy problem as well as the stochastic Burgers equation and stochastic nonlinear advection-diffusion-reaction equation. In Section 4, we summarize the present work and discuss its implications.

2 Methodology

2.1 Setup

Consider the nonlinear stochastic PDE given by:

$$\frac{\partial v}{\partial t} = f(v; x, t, \boldsymbol{\xi}), \quad (1)$$

augmented with appropriate initial and boundary conditions. In the above equation, $v = v(x, t; \boldsymbol{\xi})$, x is the spatial coordinate, $\boldsymbol{\xi} \in \mathbb{R}^d$ are the set of random parameters, t is time, and $f(v; x, t, \boldsymbol{\xi})$ includes the nonlinear spatial differential operators. We assume generic nonlinear PDEs, where the nonlinearity of f versus v may be non-polynomial, e.g., exponential, fractional, etc. For the sake of simplicity in the exposition, we consider a collocation/strong-form discretization of Eq. 1 in x and $\boldsymbol{\xi}$. Because of the simplicity of the resulting discrete system, this choice facilitates an uncluttered illustration of the main contribution of this paper, which is focused on the efficient low-rank approximation of nonlinear matrix differential equations. However, the presented methodology can also be applied to other types of discretizations, for example, weak form discretizations (finite element, etc). Examples of collocation/strong-form discretizations in the spatial domain are Fourier/polynomial spectral collocation schemes or finite-difference discretizations. Example collocation schemes in the random domain include the probabilistic collocation method (PCM) [54] or any Monte-Carlo-type sampling methods [8, 26, 32]. Applying any of the above schemes to Eq. 1 leads to the following *nonlinear matrix differential equation*:

$$\frac{d\mathbf{V}}{dt} = \mathcal{F}(t, \mathbf{V}), \quad t \in I = [0, T_f], \quad (2)$$

where $I = [0, T_f]$ denotes the time interval, $\mathbf{V}(t) : I \rightarrow \mathbb{R}^{n \times s}$ is a matrix with n rows corresponding to collocation points in the spatial domain and s columns corresponding to collocation/sampling points of the parameters $\boldsymbol{\xi}$, and $\mathcal{F}(t, \mathbf{V}) : I \times \mathbb{R}^{n \times s} \rightarrow \mathbb{R}^{n \times s}$ is obtained by discretizing $f(v; x, t, \boldsymbol{\xi})$ in x and $\boldsymbol{\xi}$. Eq. 2 is augmented with appropriate initial conditions, i.e., $\mathbf{V}(t_0) = \mathbf{V}_0$. We also assume that boundary conditions are already incorporated into Eq. 2, which can be accomplished in a number of ways, for example by using weak treatment of the boundary conditions [41].

For the remainder of this paper, we will refer to Eq. 2 as the FOM, which will be used as the ground truth for evaluating the performance of the proposed methodology. For the problems targeted in this work, we assume $n > s$ without loss of generality.

The presented methodology is limited to explicit time integration schemes. For the computational complexity analysis, we consider sparse discretization schemes for spatial discretization, which means that each row is dependent on p_a rows, where $p_a \ll n$. The

majority of discretization schemes, e.g., finite difference, finite volume, finite element, spectral element, result in sparse row dependence. As a result, the computational cost of computing each column of FOM (Eq. 2) is $\mathcal{O}(n)$ and the cost of solving MDE 2 for all s columns scales with $\mathcal{O}(ns)$. We also note that the presented methodology is *not* limited to sparse spatial discretizations and can be applied to dense discretizations as well. See Remark 2 for more details.

2.2 Preliminaries

In this section, we present some of the definitions of matrix manifolds, tangent spaces, orthogonal and oblique projections, and CUR decomposition.

Definition 1 (Low-rank matrix manifolds). *The low-rank matrix manifold \mathcal{M}_r is defined as the set*

$$\mathcal{M}_r = \{\hat{\mathbf{V}} \in \mathbb{R}^{n \times s} : \text{rank}(\hat{\mathbf{V}}) = r\},$$

of matrices of fixed rank r . Any member of the set \mathcal{M}_r is denoted by a hat symbol ($\hat{\cdot}$), e.g., $\hat{\mathbf{V}}$.

Any member of \mathcal{M}_r may be represented by $\hat{\mathbf{V}} = \mathbf{U}\mathbf{\Sigma}\mathbf{Y}^T$, where $\mathbf{U} \in \mathbb{R}^{n \times r}$ and $\mathbf{Y} \in \mathbb{R}^{s \times r}$ are a set of orthonormal columns and $\mathbf{\Sigma} \in \mathbb{R}^{r \times r}$ is a rank- r matrix. The rank- r matrix $\hat{\mathbf{V}}$ may also be represented via the multiplication of two matrices, i.e., $\hat{\mathbf{V}} = \mathbf{U}\mathbf{Y}^T$, where $\mathbf{U} \in \mathbb{R}^{n \times r}$ and $\mathbf{Y} \in \mathbb{R}^{s \times r}$ have full column rank.

Definition 2 (Tangent space). *The tangent space of manifold \mathcal{M}_r at $\hat{\mathbf{V}}$, represented with the decomposition of $\hat{\mathbf{V}} = \mathbf{U}\mathbf{\Sigma}\mathbf{Y}^T$, is the set of matrices in the form of [31]:*

$$\mathcal{T}_{\hat{\mathbf{V}}}\mathcal{M}_r = \{\delta\mathbf{U}\mathbf{\Sigma}\mathbf{Y}^T + \mathbf{U}\delta\mathbf{\Sigma}\mathbf{Y}^T + \mathbf{U}\mathbf{\Sigma}\delta\mathbf{Y}^T : \delta\mathbf{U}^T\mathbf{U} = \mathbf{0} \text{ and } \delta\mathbf{Y}^T\mathbf{Y} = \mathbf{0}\},$$

where $\delta\mathbf{U} \in \mathbb{R}^{n \times r}$ and $\delta\mathbf{Y} \in \mathbb{R}^{s \times r}$.

Definition 3 (Orthogonal projection onto the tangent space). *The orthogonal projection of matrix $\mathbf{W} \in \mathbb{R}^{n \times s}$ onto the tangent space of manifold \mathcal{M}_r at $\hat{\mathbf{V}}$, represented with the decomposition of $\hat{\mathbf{V}} = \mathbf{U}\mathbf{\Sigma}\mathbf{Y}^T$, is given by [31, Lemma 4.1]:*

$$\mathcal{P}_{\mathcal{T}_{\hat{\mathbf{V}}}}(\mathbf{W}) = \mathbf{U}\mathbf{U}^T\mathbf{W} + \mathbf{W}\mathbf{Y}\mathbf{Y}^T - \mathbf{U}\mathbf{U}^T\mathbf{W}\mathbf{Y}\mathbf{Y}^T. \quad (3)$$

In the above projection, $\mathbf{U}\mathbf{U}^T$ and $\mathbf{Y}\mathbf{Y}^T$ are orthogonal projections onto spaces spanned by the columns of \mathbf{U} and \mathbf{Y} . We denote these orthogonal projections with:

$$\mathbf{P}_{\mathbf{U}}^{\perp} = \mathbf{U}\mathbf{U}^T \quad \text{and} \quad \mathbf{P}_{\mathbf{Y}}^{\perp} = \mathbf{Y}\mathbf{Y}^T, \quad (4)$$

where the symbol \perp indicates orthogonal projection. In the following, we define oblique projectors. We first explain the notation that is used in this section. Let $\mathbf{U} \in \mathbb{R}^{n \times r}$ and $\mathbf{Y} \in \mathbb{R}^{s \times r}$ be matrices whose columns are orthonormal and let $\mathbf{p} = [p_1, p_2, \dots, p_{r'}] \in \mathbb{N}^{r'}$ and $\mathbf{s} = [s_1, s_2, \dots, s_{r'}] \in \mathbb{N}^{r'}$ be vectors containing row and column indices, where the number of indices can be greater than or equal to the dimension of the subspaces spanned by \mathbf{U} and \mathbf{Y} , i.e., $r' \geq r$. Also, $r' \leq n$ for row indices and $r' \leq s$ for column indices. We use MATLAB indexing where $\mathbf{V}(\mathbf{p}, :) \in \mathbb{R}^{r' \times s}$ selects all columns at the \mathbf{p} rows, and $\mathbf{V}(:, \mathbf{s}) \in \mathbb{R}^{n \times r'}$ selects all rows at the \mathbf{s} columns of the matrix \mathbf{V} . We also use the indexing matrices, $\mathbf{P} = \mathbf{I}_n(:, \mathbf{p}) \in \mathbb{R}^{n \times r'}$ and $\mathbf{S} = \mathbf{I}_s(:, \mathbf{s}) \in \mathbb{R}^{s \times r'}$, where \mathbf{I}_n and \mathbf{I}_s are identity matrices of size $n \times n$ and $s \times s$, respectively. It is easy to verify that $\mathbf{P}^T\mathbf{U} \equiv \mathbf{U}(\mathbf{p}, :)$ and $\mathbf{S}^T\mathbf{Y} \equiv \mathbf{Y}(\mathbf{s}, :)$. Let $(\cdot)^{\dagger}$ denote the Moore–Penrose pseudoinverse of a matrix, i.e., $\mathbf{A}^{\dagger} = (\mathbf{A}^T\mathbf{A})^{-1}\mathbf{A}^T$.

Definition 4 (Oblique projection). Let $\mathbf{U} \in \mathbb{R}^{n \times r}$ and $\mathbf{Y} \in \mathbb{R}^{s \times r}$ be orthonormal matrices and let $\mathbf{p} \in \mathbb{N}^{r'}$ and $\mathbf{s} \in \mathbb{N}^{r'}$ be sets of distinct row and column indices, respectively. Oblique projectors onto $\text{Ran}(\mathbf{U})$ and $\text{Ran}(\mathbf{Y})$ are defined as [50]

$$\mathbf{P}_{\mathbf{U}}^{\angle} = \mathbf{U}(\mathbf{P}^T \mathbf{U})^{\dagger} \mathbf{P}^T \quad \text{and} \quad \mathbf{P}_{\mathbf{Y}}^{\angle} = \mathbf{S}(\mathbf{Y}^T \mathbf{S})^{\dagger} \mathbf{Y}^T, \quad (5)$$

provided $(\mathbf{P}^T \mathbf{U})^T (\mathbf{P}^T \mathbf{U}) \in \mathbb{R}^{r \times r}$ and $(\mathbf{Y}^T \mathbf{S})^T (\mathbf{Y}^T \mathbf{S}) \in \mathbb{R}^{r \times r}$ are invertible.

In the above definition, the symbol \angle distinguishes these projectors from orthogonal projectors. For a given matrix $\mathbf{A} \in \mathbb{R}^{n \times s}$, $\mathbf{P}_{\mathbf{U}}^{\angle}$ operates on the left side of the matrix and $\mathbf{P}_{\mathbf{Y}}^{\angle}$ operates on the right side of the matrix. It is easy to verify that $(\mathbf{P}_{\mathbf{U}}^{\angle})^2 = \mathbf{P}_{\mathbf{U}}^{\angle}$ and $(\mathbf{P}_{\mathbf{Y}}^{\angle})^2 = \mathbf{P}_{\mathbf{Y}}^{\angle}$. It is also easy to verify that the oblique projection of \mathbf{A} belongs to the manifold of rank- r matrices, i.e. $\mathbf{P}_{\mathbf{U}}^{\angle} \mathbf{A} \mathbf{P}_{\mathbf{Y}}^{\angle} \in \mathcal{M}_r$.

For the special case of $r' = r$, the oblique projectors $\mathbf{P}_{\mathbf{U}}^{\angle}$ and $\mathbf{P}_{\mathbf{Y}}^{\angle}$ are also *interpolatory* projectors. In this case, the oblique projectors become $\mathbf{P}_{\mathbf{U}}^{\angle} = \mathbf{U}(\mathbf{P}^T \mathbf{U})^{-1} \mathbf{P}^T$ and $\mathbf{P}_{\mathbf{Y}}^{\angle} = \mathbf{S}(\mathbf{Y}^T \mathbf{S})^{-1} \mathbf{Y}^T$. Unlike orthogonal projection or a general oblique projection, the interpolatory projection is guaranteed to match the original matrix at the selected rows and columns, i.e.,

$$\mathbf{P}^T \mathbf{P}_{\mathbf{U}}^{\angle} \mathbf{A} = \mathbf{A}(\mathbf{p}, :) \quad \text{and} \quad \mathbf{A} \mathbf{P}_{\mathbf{Y}}^{\angle} \mathbf{S} = \mathbf{A}(:, \mathbf{s}).$$

The other extreme is when all the rows or columns are selected, i.e., $r' = n$ or $r' = s$. Take for example, the projector $\mathbf{P}_{\mathbf{U}}^{\angle}$ when $r' = n$. In this case, $\mathbf{P}_{\mathbf{U}}^{\angle}$ becomes the same as the orthogonal projector, i.e., $\mathbf{P}_{\mathbf{U}}^{\angle} \equiv \mathbf{P}_{\mathbf{U}}^{\perp}$. To show this, first note that $\mathbf{P}_{\mathbf{U}}^{\angle}$ is invariant with respect to the ordering of the row indices (\mathbf{p}) and when $r' = n$, \mathbf{p} can be taken to be: $\mathbf{p} = [1, 2, \dots, n]$. In this case, $\mathbf{P} \equiv \mathbf{I}_n$. Therefore:

$$\mathbf{P}_{\mathbf{U}}^{\angle} = \mathbf{U}(\mathbf{P}^T \mathbf{U})^{\dagger} \mathbf{P}^T = \mathbf{U}(\mathbf{U}^T \mathbf{U})^{-1} \mathbf{U}^T = \mathbf{U} \mathbf{U}^T = \mathbf{P}_{\mathbf{U}}^{\perp},$$

where we have used the orthonormality condition of \mathbf{U} , i.e., $\mathbf{U}^T \mathbf{U} = \mathbf{I}_r$, where \mathbf{I}_r is the $r \times r$ identity matrix. The analogous relationship exists for $\mathbf{P}_{\mathbf{Y}}^{\angle}$, when $r' = s$. In the following, we define CUR decompositions, which are closely related to the oblique projections.

Definition 5 (CUR decomposition). A CUR decomposition of matrix \mathbf{V} is a rank- r approximation of \mathbf{V} in the form of $\mathbf{V} \approx \mathbf{C} \mathbf{U} \mathbf{R}$, where $\mathbf{C} \in \mathbb{R}^{n \times r}$ and $\mathbf{R} \in \mathbb{R}^{r \times s}$ are actual columns and rows of matrix \mathbf{V} , i.e., $\mathbf{C} = \mathbf{V}(:, \mathbf{s})$ and $\mathbf{R} = \mathbf{V}(\mathbf{p}, :)$. The matrix $\mathbf{U} \in \mathbb{R}^{r \times r}$ is computed such that $\mathbf{C} \mathbf{U} \mathbf{R}$ is a good approximation to \mathbf{V} . The CUR of matrix \mathbf{V} is denoted with $\text{CUR}(\mathbf{V})$.

Here, the matrices, \mathbf{C} , \mathbf{U} , and \mathbf{R} are different from the matrices defined in previous sections. Different CUR decompositions can be obtained for the same matrix depending on two factors: (i) the selection of columns and rows, and (ii) the method used to compute the matrix \mathbf{U} . For more details on CUR decompositions, we refer the reader to [35]. Finally, it is easy to verify that $\text{CUR}(\mathbf{V}) \in \mathcal{M}_r$. The connection between CUR decomposition and oblique projections is shown in Section 2.7.

2.3 Time-Continuous Variational Principle

The central idea behind TDB-based low-rank approximation is that the bases evolve optimally to minimize the residual due to low-rank approximation error. The residual is

obtained by substituting an SVD-like low-rank approximation into the FOM so that $\mathbf{V}(t)$ is closely approximated by the rank- r matrix

$$\hat{\mathbf{V}}(t) = \mathbf{U}(t)\mathbf{\Sigma}(t)\mathbf{Y}(t)^T, \quad (6)$$

where $\mathbf{U}(t) \in \mathbb{R}^{n \times r}$ is a time-dependent orthonormal spatial basis for the column space, $\mathbf{Y}(t) \in \mathbb{R}^{s \times r}$ is a time-dependent orthonormal parametric basis for the row space, $\mathbf{\Sigma}(t) \in \mathbb{R}^{r \times r}$ is, in general, a full matrix, and $r \ll \min(n, s)$ is the rank of the approximation.

Because this is a low-rank approximation, it cannot satisfy the FOM exactly and there will be a residual equal to:

$$\mathbf{R}(t) = \frac{d(\mathbf{U}\mathbf{\Sigma}\mathbf{Y}^T)}{dt} - \mathcal{F}(t, \mathbf{U}\mathbf{\Sigma}\mathbf{Y}^T). \quad (7)$$

This residual is minimized via the first-order optimality conditions of the variational principle given by

$$\mathcal{J}(\dot{\mathbf{U}}, \dot{\mathbf{\Sigma}}, \dot{\mathbf{Y}}) = \left\| \frac{d(\mathbf{U}\mathbf{\Sigma}\mathbf{Y}^T)}{dt} - \mathcal{F}(t, \mathbf{U}\mathbf{\Sigma}\mathbf{Y}^T) \right\|_F^2, \quad (8)$$

subject to orthonormality constraints on \mathbf{U} and \mathbf{Y} . Since the above variational principle involves the time-continuous equation (i.e. no temporal discretization is applied), the idea is to minimize the *instantaneous* residual by optimally updating \mathbf{U} , $\mathbf{\Sigma}$, and \mathbf{Y} in time. Therefore, we refer to this as the *time-continuous* variational principle. As indicated in [31, 45], the optimality conditions of Eq. 8 lead to closed-form evolution equations for \mathbf{U} , $\mathbf{\Sigma}$, and \mathbf{Y} :

$$\dot{\mathbf{\Sigma}} = \mathbf{U}^T \mathbf{F} \mathbf{Y}, \quad (9a)$$

$$\dot{\mathbf{U}} = (\mathbf{I} - \mathbf{U}\mathbf{U}^T) \mathbf{F} \mathbf{Y} \mathbf{\Sigma}^{-1}, \quad (9b)$$

$$\dot{\mathbf{Y}} = (\mathbf{I} - \mathbf{Y}\mathbf{Y}^T) \mathbf{F}^T \mathbf{U} \mathbf{\Sigma}^{-T}, \quad (9c)$$

where $\mathbf{F} \in \mathbb{R}^{n \times s}$ is a matrix defined as $\mathbf{F} = \mathcal{F}(t, \mathbf{U}\mathbf{\Sigma}\mathbf{Y}^T)$, and \mathbf{I} is the identity matrix of appropriate dimensions. The above variational principle is the same as the Dirac–Frenkel time-dependent variational principle in the quantum chemistry literature [9] or the dynamical low-rank approximation (DLRA) [31]. In [31], the geometry of the tangent space, $\mathcal{T}_{\hat{\mathbf{V}}} \mathcal{M}_r$, was exploited to solve the constrained residual minimization problem given by Eq. 8. In this setting, the residual, $\mathcal{I}(\dot{\hat{\mathbf{V}}}) = \|\dot{\hat{\mathbf{V}}} - \mathcal{F}(t, \hat{\mathbf{V}})\|_F$, is minimized with the constraint that $\dot{\hat{\mathbf{V}}}(t) \in \mathcal{T}_{\hat{\mathbf{V}}} \mathcal{M}_r$. The solution to the above minimization problem is obtained by

$$\dot{\hat{\mathbf{V}}} = \mathcal{P}_{\mathcal{T}_{\hat{\mathbf{V}}}}(\mathcal{F}(t, \hat{\mathbf{V}})), \quad (10)$$

where $\mathcal{P}_{\mathcal{T}_{\hat{\mathbf{V}}}}$ is the orthogonal projection onto the tangent space $\mathcal{T}_{\hat{\mathbf{V}}}$ at $\hat{\mathbf{V}} = \mathbf{U}\mathbf{\Sigma}\mathbf{Y}^T$ [31, Lemma 4.1]. It is easy to show that Eqs. 9a-9c can be recovered from Eq. 10. As it was shown in [3], it is possible to derive a similar variational principle for the DO decomposition, $\hat{\mathbf{V}}(t) = \mathbf{U}_{DO}(t)\mathbf{Y}_{DO}^T(t)$, whose optimality conditions are constrained to the orthonormality of the spatial modes, $\mathbf{U}_{DO}^T \mathbf{U}_{DO} = \mathbf{I}$, via the dynamically orthogonal condition, $\dot{\mathbf{U}}_{DO}^T \mathbf{U}_{DO} = \mathbf{0}$. However, for the sake of simplicity and unlike the original DO formulation presented in [48], an evolution equation for the mean field is not derived. Without loss of generality, the low-rank DO evolution equations become

$$\dot{\mathbf{U}}_{DO} = (\mathbf{I} - \mathbf{U}_{DO} \mathbf{U}_{DO}^T) \mathbf{F} \mathbf{Y}_{DO} \mathbf{C}^{-1}, \quad (11a)$$

$$\dot{\mathbf{Y}}_{DO} = \mathbf{F}^T \mathbf{U}_{DO}, \quad (11b)$$

where $\mathbf{C} = \mathbf{Y}_{DO}^T \mathbf{Y}_{DO}$ is the low-rank correlation matrix. Note that the low-rank approximation based on DO is *equivalent* to Eq. 6, i.e., $\mathbf{U}_{DO} \mathbf{Y}_{DO}^T = \mathbf{U} \mathbf{\Sigma} \mathbf{Y}^T$. Similarly, the BO decomposition, $\hat{\mathbf{V}}(t) = \mathbf{U}_{BO}(t) \mathbf{Y}_{BO}^T(t)$, which is subject to BO conditions, $\mathbf{U}_{BO}^T \mathbf{U}_{BO} = \text{diag}(\lambda_1, \dots, \lambda_r)$ and $\mathbf{Y}_{BO}^T \mathbf{Y}_{BO} = \mathbf{I}$, is also identical to DO and Eq. 6. As it was shown in [40], one can derive matrix differential equations that transform the factorization $\{\mathbf{U}, \mathbf{\Sigma}, \mathbf{Y}\}$ to $\{\mathbf{U}_{DO}, \mathbf{Y}_{DO}\}$ or $\{\mathbf{U}_{BO}, \mathbf{Y}_{BO}\}$. The equivalence of DO and BO formulations was shown in [19]. Using the DO/BO terminology, Eqs. 9a-9c have both DO and BO conditions, i.e., the dynamically orthogonal conditions for \mathbf{U} and \mathbf{Y} : $\dot{\mathbf{U}}^T \mathbf{U} = \mathbf{0}$ and $\dot{\mathbf{Y}}^T \mathbf{Y} = \mathbf{0}$ as well as bi-orthonormality conditions: $\mathbf{U}^T \mathbf{U} = \mathbf{I}$ and $\mathbf{Y}^T \mathbf{Y} = \mathbf{I}$. Despite their equivalence, these three factorizations have different numerical performances in the presence of small singular values. As it was shown in [40], Eqs. 9a-9c outperform both DO and BO.

Despite the potential of Eqs. 9a-9c to significantly reduce the computational cost of solving massive matrix differential equations like Eq. 2, there are still a number of outstanding challenges for most practical problems of interest. As highlighted in the Introduction, computing $\mathbf{F} = \mathcal{F}(t, \mathbf{U} \mathbf{\Sigma} \mathbf{Y}^T)$ requires $\mathcal{O}(ns)$ operations that scale with the size of the FOM. This involves applying the nonlinear map (\mathcal{F}) on every column of the matrix $\hat{\mathbf{V}} = \mathbf{U} \mathbf{\Sigma} \mathbf{Y}^T$. While it is possible to achieve $\mathcal{O}(n + s)$ for the special cases of homogeneous linear and quadratic nonlinear \mathcal{F} , this comes at the expense of a highly intrusive process, that requires a careful term-by-term treatment of the right side of Eqs. 9a-9c [38, Appendix B]. Furthermore, solving Equations 9b and 9c become unstable when $\mathbf{\Sigma}$ is singular or near singular. This is particularly problematic because it is often necessary to retain very small singular values in order to have an accurate approximation.

While the low-rank approximation based on TDBs can be cast in different, yet equivalent formulations, we have chosen Eqs. 9a-9c over DO/BO/DDO decompositions to highlight the underlying challenges. Since, DO/BO/DDO decompositions exhibit all of the above challenges, addressing these challenges in the context of Eqs. 9a-9c automatically addresses the DO/BO/DDO challenges as well.

2.4 Time-Discrete Variational Principle

To address the challenges of low-rank approximations based on TDB using the time-continuous variational principle, we consider a *time-discrete* variational principle for rank-adaptive matrix approximations, which has recently been applied in [15] and also [30, 46] in the context of tensors. To this end, consider an explicit Runge-Kutta temporal discretization of Eq. 2:

$$\mathbf{V}^k = \hat{\mathbf{V}}^{k-1} + \Delta t \bar{\mathbf{F}}, \quad (12)$$

where Δt is the step size and $\bar{\mathbf{F}}$ is obtained via an explicit Euler or Runge-Kutta scheme. For example, the first-order explicit Euler method is given by: $\bar{\mathbf{F}} = \mathcal{F}(t^{k-1}, \hat{\mathbf{V}}^{k-1})$. In the above equation, it is important to note that \mathbf{V}^k is not the FOM solution since the right hand side is computed using the low-rank state from the previous time step. Despite using the rank- r $\hat{\mathbf{V}}^{k-1}$ in Eq. 12, \mathbf{V}^k will not be a rank- r matrix, i.e., $\mathbf{V}^k \notin \mathcal{M}_r$. Excluding some rare exceptions, taking one step according to Eq. 12 will put \mathbf{V}^k off the rank- r manifold. Therefore, to solve the MDE while remaining on \mathcal{M}_r , a rank truncation is needed to map the solution back onto the rank- r manifold at each time step. In other words, we need to approximate \mathbf{V}^k with a rank- r matrix, $\hat{\mathbf{V}}^k$, such that

$$\mathbf{V}^k = \hat{\mathbf{V}}^k + \mathbf{R}^k, \quad (13)$$

where \mathbf{R}^k is the low-rank approximation error.

The time-discrete variational principle can be stated as finding the best $\hat{\mathbf{V}}^k \in \mathcal{M}_r$ such that the Frobenius norm of the residual is minimized [30]:

$$\mathcal{Z}(\hat{\mathbf{V}}^k) = \left\| \mathbf{V}^k - \hat{\mathbf{V}}^k \right\|_F^2. \quad (14)$$

The solution of the above residual minimization scheme is obtained via

$$\hat{\mathbf{V}}_{best}^k = \text{SVD}(\mathbf{V}^k), \quad (15)$$

where $\text{SVD}(\mathbf{V}^k) = \mathbf{U}_{best}^k \boldsymbol{\Sigma}_{best}^k \mathbf{Y}_{best}^{kT}$ is the rank- r truncated SVD of matrix \mathbf{V}^k , where $\mathbf{U}_{best}^k \in \mathbb{R}^{n \times r}$ and $\mathbf{Y}_{best}^k \in \mathbb{R}^{s \times r}$ are the matrices of the first r left and right singular vectors of \mathbf{V}^k , respectively and $\boldsymbol{\Sigma}_{best}^k \in \mathbb{R}^{r \times r}$ is the matrix of singular values.

An important advantage of Eq. 15 over Eqs. 9a-9c is that the time advancement according to Eq. 15 does not become singular in the presence of small singular values. While this solves the issue of ill-conditioning, computing Eq. 15 at each iteration of the time stepping scheme is cost prohibitive. This computational cost is due to two sources: (i) computing the nonlinear map $\mathcal{F}(t^{k-1}, \hat{\mathbf{V}}^{k-1})$ to obtain \mathbf{V}^k and (ii) computing $\text{SVD}(\mathbf{V}^k)$. The cost of (i) alone makes the solution of the time-discrete variational principle as expensive as the FOM, i.e., $\mathcal{O}(ns)$. Besides the flops cost associated with computing \mathbf{V}^k , the memory cost of storing \mathbf{V}^k is prohibitive for most realistic applications. On the other hand, computing the exact SVD of \mathbf{V}^k scales with $\min\{\mathcal{O}(n^3), \mathcal{O}(s^3)\}$. While this cost is potentially alleviated by fast algorithms for approximating the SVD, e.g. randomized SVD [27] or incremental QR [50], for general nonlinearities in \mathcal{F} , (i) is unavoidable. This ultimately leads to a computational cost that exceeds that of the FOM.

2.5 Low-Rank Approximation via an Oblique Projection

To overcome these challenges, we present an oblique projection scheme that enables a cost-effective approximation to the rank- r $\text{SVD}(\mathbf{V}^k)$. Before presenting our methodology, we provide a geometric interpretation of $\text{SVD}(\mathbf{V}^k)$. In particular, $\text{SVD}(\mathbf{V}^k)$ can be interpreted as an orthogonal projection onto the manifold \mathcal{M}_r at $\hat{\mathbf{V}}_{best}^k$, since $\hat{\mathbf{V}}_{best}^k$ can be expressed as the orthogonal projection of \mathbf{V}^k onto the tangent space at $\hat{\mathbf{V}}_{best}^k$, i.e., $\hat{\mathbf{V}}_{best}^k = \mathcal{P}_{\mathcal{T}_{\hat{\mathbf{V}}_{best}^k}}(\mathbf{V}^k)$.

Therefore, $\hat{\mathbf{V}}_{best}^k$ can be expressed as:

$$\hat{\mathbf{V}}_{best}^k = \mathbf{P}_{\mathbf{U}_{best}^k}^L \mathbf{V}^k \mathbf{P}_{\mathbf{Y}_{best}^k}^L = \mathbf{P}_{\mathbf{U}_{best}^k}^L (\hat{\mathbf{V}}^{k-1} + \Delta t \bar{\mathbf{F}}) \mathbf{P}_{\mathbf{Y}_{best}^k}^L, \quad (16)$$

where $\mathbf{P}_{\mathbf{U}_{best}^k}^L = \mathbf{U}_{best}^k \mathbf{U}_{best}^{kT}$ and $\mathbf{P}_{\mathbf{Y}_{best}^k}^L = \mathbf{Y}_{best}^k \mathbf{Y}_{best}^{kT}$ are orthogonal projections onto the column and row space of $\hat{\mathbf{V}}_{best}^k$, respectively. The approximation $\hat{\mathbf{V}}_{best}^k$ is the optimal rank- r approximation of \mathbf{V}^k , however as mentioned in the previous section, computing $\hat{\mathbf{V}}_{best}^k$ is more expensive than solving the FOM.

In the following, we present a methodology that computes an accurate approximation to $\hat{\mathbf{V}}_{best}^k$ in a cost-effective manner. From the geometric perspective, our approach is to use an oblique projection onto a set of rank- r orthonormal column (\mathbf{U}^k) and row (\mathbf{Y}^k) subspaces:

$$\hat{\mathbf{V}}^k = \mathbf{P}_{\mathbf{U}^k}^\angle \mathbf{V}^k \mathbf{P}_{\mathbf{Y}^k}^\angle = \mathbf{P}_{\mathbf{U}^k}^\angle (\hat{\mathbf{V}}^{k-1} + \Delta t \bar{\mathbf{F}}) \mathbf{P}_{\mathbf{Y}^k}^\angle. \quad (17)$$

The above equation is analogous to Eq. 16 where the orthogonal projections are replaced with oblique projections. While orthogonal projection requires access to the entire $\hat{\mathbf{V}}^{k-1} + \Delta t \bar{\mathbf{F}}$ matrix, the oblique projectors can be designed to require the computation of $\hat{\mathbf{V}}^{k-1} + \Delta t \bar{\mathbf{F}}$ at $\mathcal{O}(r)$ columns and rows. This geometric perspective is depicted in Figure 1 panel (i).

From the matrix decomposition point of view, the above approximation may be represented via a CUR decomposition:

$$\hat{\mathbf{V}}^k = \text{CUR}(\mathbf{V}^k), \quad (18)$$

where CUR represents the algorithmic implementation of a CUR decomposition. See Figure 1 panel (iii).

From the residual minimization perspective, the SVD can be viewed as a Galerkin projection where $\|\mathbf{R}^k\|_F$ is minimized. On the other hand, the presented approach based on interpolatory projection (a special case of oblique projection) can be viewed as a *collocated* scheme where the residual is set to zero at r strategically selected rows and columns of the residual matrix, \mathbf{R}^k , in Eq. 13. To this end, we present an algorithm to set $\mathbf{R}^k(\mathbf{p}, :) = \mathbf{0}$ and $\mathbf{R}^k(:, \mathbf{s}) = \mathbf{0}$, where $\mathbf{p} \in \mathbb{N}^r$ and $\mathbf{s} \in \mathbb{N}^r$ are vectors containing the row and column indices at which the residual is set to zero. This simply requires $\hat{\mathbf{V}}^k(\mathbf{p}, :) = \mathbf{V}^k(\mathbf{p}, :)$ and $\hat{\mathbf{V}}^k(:, \mathbf{s}) = \mathbf{V}^k(:, \mathbf{s})$. See Figure 1 panel (ii). In Section 2.8, we consider oblique projection for the general case when $r' > r$ (Definition 4), where the residual at the selected rows and columns is not guaranteed to be zero.

Although the approach we will present is equivalent to the oblique projection of Eq. 17, \mathbf{U}^k and \mathbf{Y}^k are the unknown column and row bases of $\hat{\mathbf{V}}^k$ at the *current* time step. Therefore, Eq. 17 cannot be readily used for the computation of $\hat{\mathbf{V}}^k$. In the following, we present a methodology to compute these bases (and subsequently $\hat{\mathbf{V}}^k$) by strategically sampling r columns and rows of \mathbf{V}^k . While there are many possible choices for the indices \mathbf{p} and \mathbf{s} , selecting these points should be done in a principled manner, to ensure the residual at all points remains small. To compute these points, we use the discrete empirical interpolation method (DEIM) [17] which has been shown to provide near optimal sampling points for computing CUR matrix decompositions [50]. A similar approach was recently applied in [38] to accelerate the computation of Eqs. 9a-9c, by only sampling \mathbf{F} at a small number of rows and columns. However, the approach presented in [38] still suffers from the issue of ill-conditioning.

To compute the DEIM points, the rank- r SVD (or an approximation) is required [50]. Since we do not have access to the rank- r SVD at the current time step, k , we use the approximation of the SVD from the previous time step, $\hat{\mathbf{V}}^{k-1} = \mathbf{U}^{k-1} \boldsymbol{\Sigma}^{k-1} \mathbf{Y}^{k-1T}$, to compute the DEIM points. The initial approximation is ideally obtained from the FOM initial condition as the rank- r SVD(\mathbf{V}_0). The algorithm for computing $\hat{\mathbf{V}}^k$ using interpolation is as follows:

- (i) Compute the sampling indices, $\mathbf{p} \leftarrow \text{DEIM}(\mathbf{U}^{k-1})$, and $\mathbf{s} \leftarrow \text{DEIM}(\mathbf{Y}^{k-1})$, in parallel.
- (ii) Compute $\mathbf{V}^k(\mathbf{p}, :)$ and $\mathbf{V}^k(:, \mathbf{s})$ by taking one step according to Eq. 12 at the selected rows and columns, in parallel.
- (iii) Compute $\mathbf{Q} \in \mathbb{R}^{n \times r}$ as the orthonormal basis for the range of $\mathbf{V}^k(:, \mathbf{s})$ by QR decomposition such that $\mathbf{V}^k(:, \mathbf{s}) = \mathbf{QR}$, where $\mathbf{R} \in \mathbb{R}^{r \times r}$.

- (iv) Interpolate every column of \mathbf{V}^k onto the orthonormal basis \mathbf{Q} at sparse indices \mathbf{p} :

$$\mathbf{Z} = \mathbf{Q}(\mathbf{p}, :)^{-1} \mathbf{V}^k(\mathbf{p}, :), \quad (19)$$

where $\mathbf{Z} \in \mathbb{R}^{r \times s}$ is the matrix of interpolation coefficients such that \mathbf{QZ} interpolates \mathbf{V}^k onto the basis \mathbf{Q} at the interpolation points indexed by \mathbf{p} .

- (v) Compute the SVD of \mathbf{Z} so that

$$\mathbf{Z} = \mathbf{U}_Z \mathbf{\Sigma}^k \mathbf{Y}^{kT}, \quad (20)$$

where $\mathbf{U}_Z \in \mathbb{R}^{r \times r}$, $\mathbf{\Sigma}^k \in \mathbb{R}^{r \times r}$, and $\mathbf{Y}^k \in \mathbb{R}^{s \times r}$.

- (vi) Compute $\mathbf{U}^k \in \mathbb{R}^{n \times r}$ as the in-subspace rotation:

$$\mathbf{U}^k = \mathbf{Q} \mathbf{U}_Z. \quad (21)$$

In Step (i), the details of the DEIM algorithm can be found in [17, Algorithm 1]. A DEIM algorithm based on the QR factorization, a.k.a QDEIM, may also be used [23, 36]. Both DEIM and QDEIM are sparse selection algorithms and they perform comparably in the cases considered in this paper. We explain here how the above algorithm addresses the three challenges mentioned in the Introduction (1).

- (i) **Computational efficiency:** The above procedure returns the updated low-rank approximation $\hat{\mathbf{V}}^k = \mathbf{QZ} = \mathbf{U}^k \mathbf{\Sigma}^k \mathbf{Y}^{kT}$, and only requires sampling \mathbf{V}^k at r rows and columns. This alone significantly reduces both the required number of flops and memory, compared to computing the entire \mathbf{V}^k . Furthermore, instead of directly computing the SVD of the $n \times s$ matrix \mathbf{V}^k , we only require computing the QR of the $n \times r$ matrix $\mathbf{V}^k(:, \mathbf{s})$, and the SVD of the $r \times s$ matrix \mathbf{Z} . This reduces the computational cost to $\mathcal{O}(s + n)$ for $r \ll s$ and $r \ll n$. Moreover, in most practical applications, computing $\mathbf{V}^k(:, \mathbf{s})$ is the costliest part of the algorithm, which requires solving s samples of the FOM. However, since these samples are independent of each other, the columns of $\mathbf{V}^k(:, \mathbf{s})$ can be computed in parallel. Similarly, each row of $\mathbf{V}^k(\mathbf{p}, :)$ can be computed in parallel.
- (ii) **Intrusiveness:** While this significantly reduces the computational burden, perhaps an equally important outcome is the minimally intrusive nature of the above approach. For example, when the columns of \mathbf{V}^k are independent, e.g. random samples, $\mathbf{V}^k(:, \mathbf{s})$ can be computed by directly applying Eq. 12 to the selected columns of the low-rank approximation from the previous time step. This effectively allows for existing numerical implementations of Eq. 12 to be used as a black box for computing $\mathbf{V}^k(:, \mathbf{s})$. The nonintrusive column sampling in the presented algorithm is the counterpart of solving Eq. (9b) in DLRA and Eq. (11a) in DO. However, Eq. (9b) and Eq. (11a) require deriving and implementing new PDEs, whereas the presented algorithm allows an existing deterministic solver to be used in a black box fashion, in which a suitable column space basis is extracted. On the other hand, the rows of \mathbf{V}^k are in general *dependent*, based on a known map for the chosen spatial discretization scheme, e.g. sparse discretizations like finite difference, finite element, or dense discretization schemes, e.g. global spectral methods. Therefore, computing $\mathbf{V}^k(\mathbf{p}, :)$ does require specific knowledge of the governing equations, namely the discretized differential operators. Based on the discretization scheme, one can determine a set of adjacent

points, \mathbf{p}_a , that are required for computing the derivatives at the points specified by \mathbf{p} . While this introduces an added layer of complexity, this is much less intrusive than deriving and implementing reduced order operators for each term in the governing equations; which we emphasize again, is only feasible for homogeneous linear or quadratic nonlinear equations. In the present work, that bottleneck is removed, regardless of the type of nonlinearity.

- (iii) **Ill-conditioning:** The presented algorithm is robust in the presence of small or zero singular values. First note that the inversion of the matrix of singular values is not required in the presented algorithm. In fact, the conditioning of the algorithm depends on $\mathbf{Q}(\mathbf{p}, :)$ and $\mathbf{Y}(\mathbf{s}, :)$, and the DEIM algorithm ensures that these two matrices are well-conditioned. To illustrate this point, let us consider the case of overapproximation where the rank of $\mathbf{V}^k(:, \mathbf{s})$ is $r_1 < r$. In this case, Eqs. 9a-9c and Eqs. 11a-11b cannot be advanced because $\mathbf{\Sigma} \in \mathbb{R}^{r \times r}$ and $\mathbf{C} \in \mathbb{R}^{r \times r}$ will be singular, i.e., $\text{rank}(\mathbf{\Sigma}) = \text{rank}(\mathbf{C}) = r_1 < r$. On the other hand, despite $\mathbf{V}^k(:, \mathbf{s})$ being rank deficient, \mathbf{Q} will still be a full rank matrix in the presented algorithm. While there is no guarantee that a subset of rows of \mathbf{Q} , i.e., $\mathbf{Q}(\mathbf{p}, :)$ is well conditioned, the DEIM is a greedy algorithm that is designed to keep $\|\mathbf{Q}(\mathbf{p}, :)^{-1}\|$ as small as possible in a near-optimal fashion. In Section 2.8, we show that oversampling further improves the condition number of the presented algorithm, and in Theorem 3, we show that $\|\mathbf{Y}(\mathbf{s}, :)^{-1}\|$ plays an equally important role in maintaining a well-conditioned algorithm.

As we will show in Section 2.7, the low-rank approximation computed above is equivalent to a CUR matrix decomposition that interpolates \mathbf{V}^k at the selected rows and columns. Therefore, we refer to the above procedure as the TDB-CUR algorithm.

2.6 Computing $\mathbf{V}^k(\mathbf{p}, :)$

Up until this point, we have considered $\mathbf{V}^k = \hat{\mathbf{V}}^{k-1} + \Delta t \bar{\mathbf{F}}$ to be an $n \times s$ matrix resulting from an explicit Runge-Kutta temporal discretization of Eq. 12. We showed that sparse row and column measurements, $\mathbf{V}^k(\mathbf{p}, :)$ and $\mathbf{V}^k(:, \mathbf{s})$, could be used to efficiently compute an approximation to the rank- r SVD of \mathbf{V}^k . While $\mathbf{V}^k(:, \mathbf{s})$ is straightforward to compute for independent random samples, as discussed in Section 2.5, computing $\mathbf{V}^k(\mathbf{p}, :)$ depends on a set of adjacent points, \mathbf{p}_a , according to the spatial discretization scheme. As a result, for higher-order integration schemes, special care must be taken in the computation of $\mathbf{V}^k(\mathbf{p}, :)$. To demonstrate this, we consider the second-order explicit Runge-Kutta scheme where

$$\bar{\mathbf{F}} = \mathcal{F} \left(t^{k-1} + \frac{1}{2} \Delta t, \hat{\mathbf{V}}^{k-1} + \frac{1}{2} \Delta t \mathcal{F} \left(t^{k-1}, \hat{\mathbf{V}}^{k-1} \right) \right)$$

After determining the row indices, \mathbf{p} and \mathbf{p}_a , $\mathbf{V}^k(\mathbf{p}, :)$ can be computed as follows:

- (i) Compute $\hat{\mathbf{V}}^{k-1}([\mathbf{p}, \mathbf{p}_a], :) = \mathbf{U}^{k-1}([\mathbf{p}, \mathbf{p}_a], :)\mathbf{\Sigma}^{k-1}\mathbf{Y}^{k-1T}$.
- (ii) Compute the first stage $\mathbf{F}_1 = \mathcal{F} \left(t^{k-1}, \hat{\mathbf{V}}^{k-1} \right)$ at the \mathbf{p} rows as

$$\mathbf{F}_1(\mathbf{p}, :) = \mathcal{F} \left(t^{k-1}, \hat{\mathbf{V}}^{k-1}([\mathbf{p}, \mathbf{p}_a], :) \right).$$

Note, if the explicit Euler method is used, $\bar{\mathbf{F}} = \mathbf{F}_1$, and no additional steps are required. Simply compute $\mathbf{V}^k(\mathbf{p}, :) = \hat{\mathbf{V}}^{k-1} + \Delta t \mathbf{F}_1(\mathbf{p}, :)$. If a higher-order scheme is used, proceed with the following steps.

- (iii) The final stage of the second order integration scheme requires taking a half step to evaluate \mathcal{F} at the midpoint:

$$\mathbf{F}_2 = \mathcal{F} \left(t^{k-1} + \frac{1}{2} \Delta t, \hat{\mathbf{V}}^{k-1} + \frac{1}{2} \Delta t \mathbf{F}_1 \right).$$

Note that for the second order scheme, $\bar{\mathbf{F}} = \mathbf{F}_2$. Here, we require $\mathbf{F}_2(\mathbf{p}, :)$, given by

$$\mathbf{F}_2(\mathbf{p}, :) = \mathcal{F} \left(t^{k-1} + \frac{1}{2} \Delta t, \hat{\mathbf{V}}^{k-1}([\mathbf{p}, \mathbf{p}_a], :) + \frac{1}{2} \Delta t \mathbf{F}_1([\mathbf{p}, \mathbf{p}_a], :) \right).$$

Notice that we now require $\mathbf{F}_1(\mathbf{p}_a, :)$ to evaluate the above expression. While this can be computed according to Step (ii), where \mathbf{p}_a will have its own set of adjacent points \mathbf{p}_{aa} , this process quickly gets out of hand, especially as more stages are added to the integration scheme. As a result, for higher-order schemes, the efficiency afforded by the presented algorithm will deteriorate, and the resulting implementation will become increasingly complex. To overcome these challenges, we instead compute the low-rank approximation $\hat{\mathbf{F}}_i \approx \mathbf{F}_i$, using the sparse row and column measurements, $\mathbf{F}_i(\mathbf{p}, :)$ and $\mathbf{F}_i(:, \mathbf{s})$, which are already required for computing $\mathbf{V}^k(\mathbf{p}, :)$ and $\mathbf{V}^k(:, \mathbf{s})$. Here, the subscript denotes the i^{th} stage of the integration scheme. The first step is to compute $\mathbf{U}_{\mathbf{F}_i}$ as an orthonormal basis for the $\text{Ran}(\mathbf{F}_i(:, \mathbf{s}))$, using QR. Next, compute the oblique projection of \mathbf{F}_i onto $\mathbf{U}_{\mathbf{F}_i}$, such that

$$\hat{\mathbf{F}}_i = \mathbf{U}_{\mathbf{F}_i} \mathbf{U}_{\mathbf{F}_i}(\mathbf{p}, :)^{-1} \mathbf{F}_i(\mathbf{p}, :).$$

Using this low-rank approximation, $\mathbf{F}_i(\mathbf{p}_a, :)$ is readily approximated by $\hat{\mathbf{F}}_i(\mathbf{p}_a, :) = \mathbf{U}_{\mathbf{F}_i}(\mathbf{p}_a, :)^{-1} \mathbf{F}_i(\mathbf{p}, :)$. Although we have considered the second-order Runge-Kutta method in the example above, this approach is easily extended to higher-order Runge-Kutta methods. It is straightforward to show that the above procedure is equivalent to a CUR decomposition of matrix \mathbf{F}_i , similar to our previous work [38].

2.7 Equivalence to a CUR Decomposition & Oblique Projection

Before presenting the details of our methodology in Section 2.5, we discussed how the presented approach can be understood as an oblique projection (Eq. 17) or alternatively as a CUR decomposition (Eq. 18). In this section, we show that (i) the presented algorithm is equivalent to a CUR decomposition (Theorem 1), and (ii) the matrix $\hat{\mathbf{V}}^k$ is obtained via an oblique projection, which requires access to only the selected rows and columns of \mathbf{V}^k (Theorem 2). In Theorem 1 and Theorem 2, \mathbf{P} and \mathbf{S} are matrices of size $n \times r$ and $s \times r$, respectively. We drop the time step k for simplicity.

Theorem 1. *Let $\hat{\mathbf{V}} = \mathbf{QZ}$ be the low-rank approximation of \mathbf{V} computed according to the TDB-CUR algorithm. Then: (i) $\hat{\mathbf{V}} = \mathbf{QZ}$ is equivalent to the CUR factorization given by $(\mathbf{VS})(\mathbf{P}^T \mathbf{VS})^{-1}(\mathbf{P}^T \mathbf{V})$. (ii) The low-rank approximation is exact at the selected rows and columns, i.e. $\mathbf{P}^T \hat{\mathbf{V}} = \mathbf{P}^T \mathbf{V}$ and $\hat{\mathbf{V}} \mathbf{S} = \mathbf{V} \mathbf{S}$.*

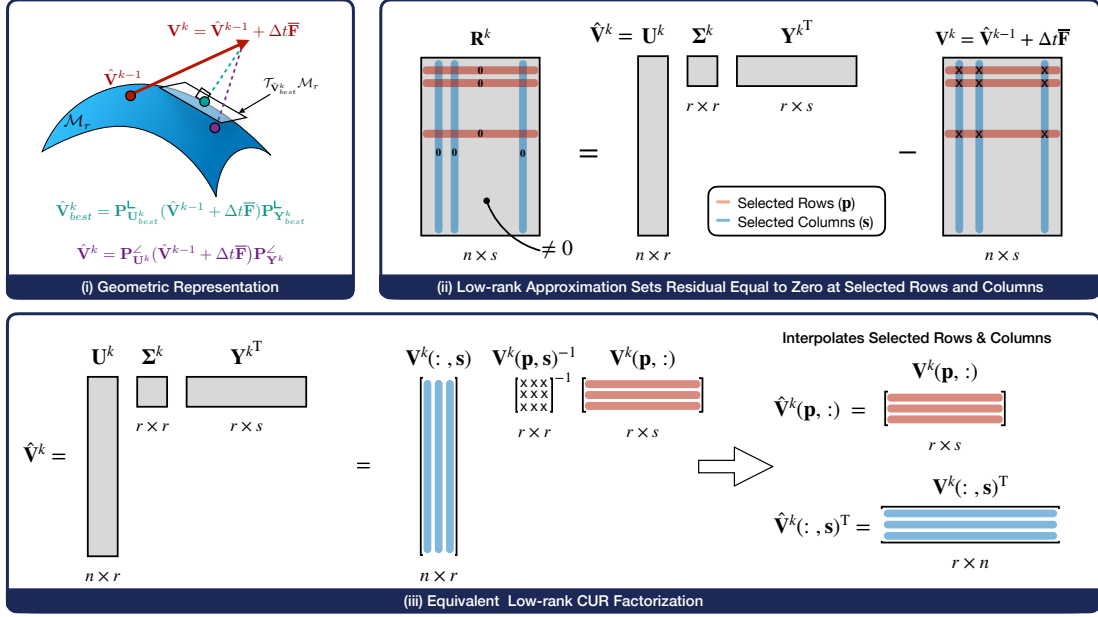


Figure 1: Schematic of the TDB-CUR methodology. (i) A geometric representation of the methodology depicting the departure from the rank- r manifold at $\hat{\mathbf{V}}^{k-1}$ to \mathbf{V}^k (red). Two possible mappings that truncate \mathbf{V}^k back to the rank- r manifold are shown: $\hat{\mathbf{V}}_{best}^k$ (green) computed via orthogonal projection (SVD) and $\hat{\mathbf{V}}^k$ (purple) computed via oblique projection (TDB-CUR). The error of $\hat{\mathbf{V}}_{best}^k$ (dashed green line) is orthogonal to the tangent space $\mathcal{T}_{\hat{\mathbf{V}}_{best}^k} \mathcal{M}_r$ at $\hat{\mathbf{V}}_{best}^k$, while the error of $\hat{\mathbf{V}}^k$ (dashed purple line) is not. (ii) The low-rank approximation, $\hat{\mathbf{V}}^k$, can be computed such that the residual at the selected rows (red) and columns (blue) is equal to zero. This is accomplished via sparse interpolation of the selected rows and columns. (iii) Using interpolatory projection, the resulting $\hat{\mathbf{V}}^k$ is an approximation to the rank- r truncated $\text{SVD}(\mathbf{V}^k)$, and is equivalent to the low-rank CUR factorization that interpolates the selected rows and columns of \mathbf{V}^k . Although it is equivalent to this CUR factorization, the numerical computation of $\hat{\mathbf{V}}^k$ is different, as it does not require inverting $\mathbf{V}^k(\mathbf{p}, \mathbf{s})$.

Proof.

(i) According to the TDB-CUR algorithm, \mathbf{Q} is a basis for the $\text{Ran}(\mathbf{V}(:, \mathbf{s}))$. Therefore, $\mathbf{V}(:, \mathbf{s}) = \mathbf{V}\mathbf{S} = \mathbf{Q}\mathbf{Q}^T\mathbf{V}\mathbf{S}$, and it follows that $\mathbf{P}^T\mathbf{V}\mathbf{S} = \mathbf{P}^T\mathbf{Q}\mathbf{Q}^T\mathbf{V}\mathbf{S}$. Substituting this result into the CUR factorization gives

$$(\mathbf{V}\mathbf{S})(\mathbf{P}^T\mathbf{V}\mathbf{S})^{-1}(\mathbf{P}^T\mathbf{V}) = \mathbf{Q}\mathbf{Q}^T\mathbf{V}\mathbf{S}(\mathbf{P}^T\mathbf{Q}\mathbf{Q}^T\mathbf{V}\mathbf{S})^{-1}\mathbf{P}^T\mathbf{V}.$$

Rearranging the above expression gives the desired result

$$(\mathbf{V}\mathbf{S})(\mathbf{P}^T\mathbf{V}\mathbf{S})^{-1}(\mathbf{P}^T\mathbf{V}) = \mathbf{Q}\mathbf{Q}^T\mathbf{V}\mathbf{S}(\mathbf{Q}^T\mathbf{V}\mathbf{S})^{-1}(\mathbf{P}^T\mathbf{Q})^{-1}\mathbf{P}^T\mathbf{V} = \mathbf{Q}\mathbf{Z} = \hat{\mathbf{V}},$$

where we have used $\mathbf{Z} = (\mathbf{P}^T\mathbf{Q})^{-1}\mathbf{P}^T\mathbf{V} = \mathbf{Q}(\mathbf{p}, :)^{-1}\mathbf{V}(\mathbf{p}, :)$, from Eq. 19.

(ii) Using the above result, $\hat{\mathbf{V}} = (\mathbf{V}\mathbf{S})(\mathbf{P}^T\mathbf{V}\mathbf{S})^{-1}(\mathbf{P}^T\mathbf{V})$, we show the selected rows of $\hat{\mathbf{V}}$ are exact, i.e., $\hat{\mathbf{V}}(\mathbf{p}, :) = \mathbf{V}(\mathbf{p}, :)$:

$$\mathbf{P}^T\hat{\mathbf{V}} = (\mathbf{P}^T\mathbf{V}\mathbf{S})(\mathbf{P}^T\mathbf{V}\mathbf{S})^{-1}(\mathbf{P}^T\mathbf{V}) = \mathbf{P}^T\mathbf{V}.$$

Similarly for the columns,

$$\hat{\mathbf{V}}\mathbf{S} = (\mathbf{V}\mathbf{S})(\mathbf{P}^T\mathbf{V}\mathbf{S})^{-1}(\mathbf{P}^T\mathbf{V}\mathbf{S}) = \mathbf{V}\mathbf{S}.$$

This completes the proof. □

Now we show that $\hat{\mathbf{V}}$ is an oblique projection of \mathbf{V} onto the selected columns and rows of \mathbf{V} . In particular, the oblique projector involved is an interpolatory projector. For the sake of brevity, we drop the superscript k in the following.

Theorem 2. Let $\hat{\mathbf{V}} = \mathbf{Q}\mathbf{Z}$ be the low-rank approximation of \mathbf{V} computed according to the TDB-CUR algorithm. Then $\hat{\mathbf{V}} = \mathbf{P}_U^\angle \mathbf{V} \mathbf{P}_Y^\angle$ where \mathbf{P}_U^\angle and \mathbf{P}_Y^\angle are oblique projectors onto $\text{Ran}(\mathbf{U})$ and $\text{Ran}(\mathbf{Y})$, respectively, according to Eq. 5.

Proof. We first show that \mathbf{P}_U^\angle can be represented versus \mathbf{Q} as the interpolation basis. To this end, replacing $\mathbf{U} = \mathbf{Q}\mathbf{U}_Z$ in the definition of \mathbf{P}_U^\angle results in:

$$\mathbf{P}_U^\angle = \mathbf{U}(\mathbf{P}^T\mathbf{U})^{-1}\mathbf{P}^T = \mathbf{Q}\mathbf{U}_Z(\mathbf{P}^T\mathbf{Q}\mathbf{U}_Z)^{-1}\mathbf{P}^T = \mathbf{Q}\mathbf{U}_Z\mathbf{U}_Z^{-1}(\mathbf{P}^T\mathbf{Q})^{-1}\mathbf{P}^T = \mathbf{Q}(\mathbf{P}^T\mathbf{Q})^{-1}\mathbf{P}^T.$$

where we have used the fact that \mathbf{U}_Z is a square orthonormal matrix and therefore, $\mathbf{U}_Z\mathbf{U}_Z^{-1} = \mathbf{I}$. Similarly, \mathbf{P}_Y^\angle can be represented versus \mathbf{Z}^T as the interpolation basis by replacing $\mathbf{Y}^T = \Sigma^{-1}\mathbf{U}_Z^{-1}\mathbf{Z}$ in \mathbf{P}_Y^\angle :

$$\mathbf{P}_Y^\angle = \mathbf{S}(\mathbf{Y}^T\mathbf{S})^{-1}\mathbf{Y}^T = \mathbf{S}(\Sigma^{-1}\mathbf{U}_Z^{-1}\mathbf{Z}\mathbf{S})^{-1}\Sigma^{-1}\mathbf{U}_Z^{-1}\mathbf{Z} = \mathbf{S}(\mathbf{Z}\mathbf{S})^{-1}\mathbf{Z}.$$

Using these projection operators we have

$$\mathbf{P}_U^\angle \mathbf{V} \mathbf{P}_Y^\angle = \mathbf{Q}(\mathbf{P}^T\mathbf{Q})^{-1}\mathbf{P}^T\mathbf{V}\mathbf{S}(\mathbf{Z}\mathbf{S})^{-1}\mathbf{Z}. \quad (22)$$

Using the results of Theorem 1, Part (ii), we have: $\mathbf{V}(\mathbf{p}, \mathbf{s}) = \hat{\mathbf{V}}(\mathbf{p}, \mathbf{s})$. Therefore:

$$\mathbf{P}^T\mathbf{V}\mathbf{S} = \mathbf{V}(\mathbf{p}, \mathbf{s}) = \hat{\mathbf{V}}(\mathbf{p}, \mathbf{s}) = \mathbf{Q}(\mathbf{p}, :)\mathbf{Z}(:, \mathbf{s}) = \mathbf{P}^T\mathbf{Q}\mathbf{Z}\mathbf{S}.$$

Using this result in Eq. 22, yields:

$$\mathbf{P}_U^\angle \mathbf{V} \mathbf{P}_Y^\angle = \mathbf{Q}(\mathbf{P}^T\mathbf{Q})^{-1}\mathbf{P}^T\mathbf{Q}\mathbf{Z}\mathbf{S}(\mathbf{Z}\mathbf{S})^{-1}\mathbf{Z} = \mathbf{Q}\mathbf{Z} = \hat{\mathbf{V}}.$$

This result completes the proof. □

In the following theorem, we show that the oblique projection error is bounded by an error factor multiplied by the maximum of orthogonal projection errors onto \mathbf{U} or \mathbf{Y} . We follow a similar procedure that was used in [50], however, in [50] the CUR is computed based on orthogonal projections onto the selected columns and rows, whereas in the presented TDB-CUR algorithm, oblique projectors are used. Without loss of generality, we consider a generic oblique projection, where the indexing matrices \mathbf{P} and \mathbf{S} are of size $n \times r'$ and $s \times r'$, respectively, and in general, $r' \geq r$ (see Definition 4 for details). In the following, we use the second norm ($\|\sim\| \equiv \|\sim\|_2$).

Theorem 3. *Let $\mathbf{P}_\mathbf{U}^\prec$ and $\mathbf{P}_\mathbf{Y}^\prec$ be oblique projectors according to Definition 4 and let $\mathbf{U} \in \mathbb{R}^{n \times r}$ and $\mathbf{Y} \in \mathbb{R}^{s \times r}$ be a set of orthonormal matrices, i.e., $\mathbf{U}^T \mathbf{U} = \mathbf{I}$ and $\mathbf{Y}^T \mathbf{Y} = \mathbf{I}$. Let $\epsilon_f \geq 0$ be given by: $\epsilon_f = \min\{\eta_p(1 + \eta_s), \eta_s(1 + \eta_p)\} - 1$, where $\eta_p = \|(\mathbf{P}^T \mathbf{U})^\dagger\|$ and $\eta_s = \|(\mathbf{S}^T \mathbf{Y})^\dagger\|$ and $\hat{\sigma}_{r+1} = \max\{\|\mathbf{V} - \mathbf{U}\mathbf{U}^T \mathbf{V}\|, \|\mathbf{V} - \mathbf{V}\mathbf{Y}\mathbf{Y}^T\|\}$. Then the error of the oblique projection is bounded by*

$$\|\mathbf{V} - \mathbf{P}_\mathbf{U}^\prec \mathbf{V} \mathbf{P}_\mathbf{Y}^\prec\| \leq (1 + \epsilon_f) \hat{\sigma}_{r+1}. \quad (23)$$

Proof. First note that $\epsilon_f \geq 0$ because $\eta_p \geq 1$ and $\eta_s \geq 1$. The error matrix can be written as:

$$\mathbf{V} - \mathbf{P}_\mathbf{U}^\prec \mathbf{V} \mathbf{P}_\mathbf{Y}^\prec = (\mathbf{I} - \mathbf{P}_\mathbf{U}^\prec) \mathbf{V} + \mathbf{P}_\mathbf{U}^\prec \mathbf{V} - \mathbf{P}_\mathbf{U}^\prec \mathbf{V} \mathbf{P}_\mathbf{Y}^\prec = (\mathbf{I} - \mathbf{P}_\mathbf{U}^\prec) \mathbf{V} + \mathbf{P}_\mathbf{U}^\prec \mathbf{V} (\mathbf{I} - \mathbf{P}_\mathbf{Y}^\prec)$$

where \mathbf{I} is the identity matrix of appropriate size. Also, $\mathcal{P}\mathbf{U} = \mathbf{U}(\mathbf{P}^T \mathbf{U})^{-1} \mathbf{P}^T \mathbf{U} = \mathbf{U}$. Therefore, $(\mathbf{I} - \mathbf{P}_\mathbf{U}^\prec) \mathbf{U} = \mathbf{0}$. Similarly, $\mathbf{Y}^T (\mathbf{I} - \mathbf{P}_\mathbf{Y}^\prec) = \mathbf{0}$. Therefore,

$$\begin{aligned} \|\mathbf{V} - \mathbf{P}_\mathbf{U}^\prec \mathbf{V} \mathbf{P}_\mathbf{Y}^\prec\| &\leq \|(\mathbf{I} - \mathbf{P}_\mathbf{U}^\prec) \mathbf{V}\| + \|\mathbf{P}_\mathbf{U}^\prec \mathbf{V} (\mathbf{I} - \mathbf{P}_\mathbf{Y}^\prec)\| \\ &= \|(\mathbf{I} - \mathbf{P}_\mathbf{U}^\prec) (\mathbf{V} - \mathbf{U} \mathbf{U}^T \mathbf{V})\| + \|\mathbf{P}_\mathbf{U}^\prec (\mathbf{V} - \mathbf{V} \mathbf{Y} \mathbf{Y}^T) (\mathbf{I} - \mathbf{P}_\mathbf{Y}^\prec)\| \\ &\leq (\|(\mathbf{I} - \mathbf{P}_\mathbf{U}^\prec)\| + \|\mathbf{P}_\mathbf{U}^\prec\| \|(\mathbf{I} - \mathbf{P}_\mathbf{Y}^\prec)\|) \hat{\sigma}_{r+1} \\ &= \eta_p (1 + \eta_s) \hat{\sigma}_{r+1}. \end{aligned}$$

In the above inequality, we have made use of the fact that $\|\mathbf{I} - \mathbf{P}_\mathbf{U}^\prec\| = \|\mathbf{P}_\mathbf{U}^\prec\| = \eta_p$ and $\|\mathbf{I} - \mathbf{P}_\mathbf{Y}^\prec\| = \|\mathbf{P}_\mathbf{Y}^\prec\| = \eta_s$ as long as the projectors are neither null nor the identity [51]. In the second line of the above inequality, we have made use of $(\mathbf{I} - \mathbf{P}_\mathbf{U}^\prec) \mathbf{U} = \mathbf{0}$ and $\mathbf{Y}^T (\mathbf{I} - \mathbf{P}_\mathbf{Y}^\prec) = \mathbf{0}$. Similarly, it is possible to express the error matrix as:

$$\mathbf{V} - \mathbf{P}_\mathbf{U}^\prec \mathbf{V} \mathbf{P}_\mathbf{Y}^\prec = \mathbf{V} (\mathbf{I} - \mathbf{P}_\mathbf{Y}^\prec) + \mathbf{V} \mathbf{P}_\mathbf{Y}^\prec - \mathbf{P}_\mathbf{U}^\prec \mathbf{V} \mathbf{P}_\mathbf{Y}^\prec = \mathbf{V} (\mathbf{I} - \mathbf{P}_\mathbf{Y}^\prec) + (\mathbf{I} - \mathbf{P}_\mathbf{U}^\prec) \mathbf{V} \mathbf{P}_\mathbf{Y}^\prec.$$

Therefore, another error bound can be obtained as

$$\begin{aligned} \|\mathbf{V} - \mathbf{P}_\mathbf{U}^\prec \mathbf{V} \mathbf{P}_\mathbf{Y}^\prec\| &\leq \|\mathbf{V} (\mathbf{I} - \mathbf{P}_\mathbf{Y}^\prec)\| + \|(\mathbf{I} - \mathbf{P}_\mathbf{U}^\prec) \mathbf{V} \mathbf{P}_\mathbf{Y}^\prec\| \\ &= \|(\mathbf{V} - \mathbf{V} \mathbf{Y} \mathbf{Y}^T) (\mathbf{I} - \mathbf{P}_\mathbf{Y}^\prec)\| + \|(\mathbf{I} - \mathbf{P}_\mathbf{U}^\prec) (\mathbf{V} - \mathbf{U} \mathbf{U}^T \mathbf{V}) \mathbf{P}_\mathbf{Y}^\prec\| \\ &\leq (\|(\mathbf{I} - \mathbf{P}_\mathbf{Y}^\prec)\| + \|\mathbf{I} - \mathbf{P}_\mathbf{U}^\prec\| \|\mathbf{P}_\mathbf{Y}^\prec\|) \hat{\sigma}_{r+1} \\ &= \eta_s (1 + \eta_p) \hat{\sigma}_{r+1}. \end{aligned}$$

where $\|\mathbf{I} - \mathbf{P}_\mathbf{Y}^\prec\| = \eta_s$ is used. Combining the above two inequalities yields inequality 23. \square

In the above error bound, when \mathbf{U} and \mathbf{Y} are the r most dominant exact left and right singular vectors of \mathbf{V} , then $\hat{\sigma}_{r+1} = \sigma_{r+1}$, where σ_{r+1} is the $r + 1$ -th singular value of \mathbf{V} , since

$$\|\mathbf{V} - \mathbf{U} \mathbf{U}^T \mathbf{V}\| = \|\mathbf{V} - \mathbf{V} \mathbf{Y} \mathbf{Y}^T\| = \sigma_{r+1}. \quad (24)$$

In that case, $1 + \epsilon_f$ is the error factor of the CUR decomposition when compared against the optimal rank- r reduction error obtained by SVD. As demonstrated in our numerical experiments, the TDB-CUR algorithm closely approximates the rank- r SVD approximation of \mathbf{V} .

2.8 Oversampling for Improved Condition Number

The above error analysis shows that the CUR rank- r approximation can be bounded by an error factor ϵ_f times the maximum error obtained from the orthogonal projection of \mathbf{V} onto \mathbf{U} or \mathbf{Y} . This analysis reveals that better conditioned $\mathbf{P}^T \mathbf{U}$ and $\mathbf{S}^T \mathbf{Y}$ matrices result in smaller η_p and η_s , which then results in smaller error factor ϵ_f . In the context of DEIM interpolation, it was shown that *oversampling* can improve the condition number of oblique projections [56]. The authors demonstrated that augmenting the original DEIM algorithm with an additional $m = \mathcal{O}(r)$ sampling points can reduce the value of η_p , leading to smaller approximation errors. This procedure of sampling more rows than the number of basis vectors leads to an overdetermined system where an approximate solution can be found via a least-square regression rather than interpolation. Additionally, it was shown in [2] that for matrices with rapidly decaying singular values (as targeted in this work), oversampling improves the accuracy of CUR decompositions.

In the following, we extend the TDB-CUR algorithm for row oversampling. As a direct result of the oversampling procedure, the oblique projection of \mathbf{V} onto the range of the orthonormal basis \mathbf{Q} becomes:

$$\mathbf{Z} = \mathbf{Q}(\mathbf{p}, :)^{\dagger} \mathbf{V}(\mathbf{p}, :), \quad \text{where} \quad \mathbf{Q}(\mathbf{p}, :)^{\dagger} = (\mathbf{Q}(\mathbf{p}, :)^T \mathbf{Q}(\mathbf{p}, :))^{-1} \mathbf{Q}(\mathbf{p}, :)^T, \quad (25)$$

and $\mathbf{p} \in \mathbb{N}^{r'}$ contains the $r' = r + m \ll n$ row indices. Note that $\mathbf{Q}(\mathbf{p}, :)^{\dagger}$ is the pseudo-inverse of $\mathbf{Q}(\mathbf{p}, :)$, however, we do not apply any singular value threshold cutoff to compute $\mathbf{Q}(\mathbf{p}, :)^{\dagger}$ and exact inversion of $\mathbf{Q}(\mathbf{p}, :)^T \mathbf{Q}(\mathbf{p}, :)$ is used. Therefore, the oblique projection becomes a least squares best-fit solution. Also, increasing the number of oversampling points decreases $\eta_p = \|\mathbf{Q}(\mathbf{p}, :)^{\dagger}\|$ and it follows that for the maximum number of oversampling points, i.e., when all the rows are sampled, the orthogonal projection of every column of \mathbf{V} onto $\text{Ran}(\mathbf{V}(:, \mathbf{s}))$ is recovered, where η_p attains its smallest value, which is $\eta_p = 1$. Note that, unlike the interpolatory projector, $\mathbf{P}^T \mathbf{P}_{\mathbf{U}}^{\perp} \mathbf{A} \neq \mathbf{A}(\mathbf{p}, :)$. The oversampling is also applied analogously to the CUR decomposition of \mathbf{F} :

$$\hat{\mathbf{F}}_i = \mathbf{U}_{\mathbf{F}_i} \mathbf{U}_{\mathbf{F}_i}(\mathbf{p}, :)^{\dagger} \mathbf{F}_i(\mathbf{p}, :),$$

where $\mathbf{U}_{\mathbf{F}_i}(\mathbf{p}, :)^{\dagger} = (\mathbf{U}_{\mathbf{F}_i}(\mathbf{p}, :)^T \mathbf{U}_{\mathbf{F}_i}(\mathbf{p}, :))^{-1} \mathbf{U}_{\mathbf{F}_i}(\mathbf{p}, :)^T$. The CUR approximation of \mathbf{F} is presented in Section 2.6.

We refer to the above sampling procedure as OS-DEIM, where OS refers to the oversampling algorithm. Since the DEIM only provides sampling points equal to the number of basis vectors, we use the GappyPOD+E algorithm from [44] to sample a total of r' rows. For convenience, the algorithm is provided in Listing 2. While any sparse selection procedure can be used, the GappyPOD+E was shown to outperform other common choices like random sampling or leverage scores [35]. Finally, it is possible to oversample the columns in an analogous manner to decrease η_s . In all of the examples considered in this paper, we apply row oversampling, but ultimately the decision for row oversampling, column oversampling, or both may be made by requiring that η_p and η_s be smaller than some threshold values.

Algorithm 1 Rank-Adaptive TDB-CUR Algorithm

Input: $\tilde{\mathbf{U}} \in \mathbb{R}^{n \times \tilde{r}}$, $\tilde{\Sigma} \in \mathbb{R}^{\tilde{r} \times \tilde{r}}$, $\tilde{\mathbf{Y}} \in \mathbb{R}^{s \times \tilde{r}}$, \tilde{r} , m (\sim indicates quantities from previous time step)

Output: $\mathbf{U} \in \mathbb{R}^{n \times r}$, $\Sigma \in \mathbb{R}^{r \times r}$, $\mathbf{Y} \in \mathbb{R}^{s \times r}$, r

```
1:  $\epsilon = \tilde{\Sigma}(\tilde{r}, \tilde{r}) / \|\text{diag}(\tilde{\Sigma})\|_2$   $\triangleright$  Compute error proxy for adaptive rank criteria.
2: if  $\epsilon > \epsilon_u$  then  $\triangleright$  Increase rank if  $\epsilon$  exceeds the upper threshold,  $\epsilon_u$ .
3:    $r = \tilde{r} + 1$ 
4: else if  $\epsilon < \epsilon_l$  then  $\triangleright$  Decrease rank if  $\epsilon$  falls below the lower threshold,  $\epsilon_l$ .
5:    $r = \tilde{r} - 1$ 
6:    $\tilde{\mathbf{U}} = \tilde{\mathbf{U}}(:, 1:r)$ ;  $\tilde{\Sigma} = \tilde{\Sigma}(1:r, 1:r)$ ;  $\tilde{\mathbf{Y}} = \tilde{\mathbf{Y}}(:, 1:r)$   $\triangleright$  Truncate TDB matrices.
7: else  $\triangleright$  Keep rank the same.
8:    $r = \tilde{r}$ 
9: end if
10:  $\mathbf{s} \leftarrow \text{sparse\_selection}(\tilde{\mathbf{Y}}, r)$   $\triangleright$  Compute  $r$  column indices.
11:  $\mathbf{p} \leftarrow \text{sparse\_selection}(\tilde{\mathbf{U}}, r + m)$   $\triangleright$  Compute  $r + m$  row indices.
12:  $\mathbf{p}_a \leftarrow \text{find\_adjacent}(\mathbf{p})$   $\triangleright$  Find adjacent points required to compute  $\mathbf{V}(\mathbf{p}, :)$ .
13:  $\hat{\mathbf{V}}(:, \mathbf{s}) = \tilde{\mathbf{U}}\tilde{\Sigma}\tilde{\mathbf{Y}}(\mathbf{s}, :)^T$   $\triangleright$  Construct low-rank approximation of columns in  $\mathbf{s}$ .
14:  $\mathbf{V}(:, \mathbf{s}) = \hat{\mathbf{V}}(:, \mathbf{s}) + \Delta t \bar{\mathbf{F}}(:, \mathbf{s})$   $\triangleright$  Take one step at the selected columns.
15:  $\hat{\mathbf{V}}([\mathbf{p}, \mathbf{p}_a], :) = \tilde{\mathbf{U}}([\mathbf{p}, \mathbf{p}_a], :)\tilde{\Sigma}\tilde{\mathbf{Y}}^T$   $\triangleright$  Construct low-rank approximation of rows in  $[\mathbf{p}, \mathbf{p}_a]$ .
16:  $\mathbf{V}(\mathbf{p}, :) = \hat{\mathbf{V}}(\mathbf{p}, :) + \Delta t \bar{\mathbf{F}}(\mathbf{p}, :)$   $\triangleright$  Take one step at the selected rows.
17:  $\mathbf{QR} = \text{QR}(\mathbf{V}(:, \mathbf{s}), \text{'econ'})$   $\triangleright$  Compute the economy QR of  $\mathbf{V}(:, \mathbf{s})$ .
18:  $\mathbf{Z} = \mathbf{Q}(\mathbf{p}, :)^{\dagger} \mathbf{V}(\mathbf{p}, :)$   $\triangleright$  Compute  $\mathbf{Z}$  as an oblique projection of  $\mathbf{V}$  onto  $\mathbf{Q}$ .
19:  $\mathbf{U}_Z \Sigma \mathbf{Y}^T = \text{SVD}(\mathbf{Z}, \text{'econ'})$   $\triangleright$  Compute the economy SVD of  $\mathbf{Z}$ .
20:  $\mathbf{U} = \mathbf{Q} \mathbf{U}_Z$   $\triangleright$  In-subspace rotation of the orthonormal basis,  $\mathbf{Q}$ .
```

^aWhile the present work uses the GappyPOD+E for `sparse_selection`, the user is free to choose their favorite sparse selection algorithm.

2.9 Rank Adaptivity

In order to control the error while avoiding unnecessary computations, the rank of the TDB must be able to adapt on the fly. The importance of rank adaptivity for low-rank approximation with TDB has been recognized and several algorithms have been proposed recently. See for example [14, 20, 55]. We show that it is easy to incorporate mode adaptivity into the TDB-CUR algorithm. In the case of rank reduction, once the new rank is chosen, such that $r^k < r^{k-1}$, the low-rank matrices are simply truncated to retain only the first r^k components, i.e. $\mathbf{U}(:, 1:r^k)$, $\Sigma(1:r^k, 1:r^k)$, and $\mathbf{Y}(:, 1:r^k)$. On the other hand, the rank can be increased, such that $r^k > r^{k-1}$, by sampling more columns (r^k) than the number of basis vectors (r^{k-1}), i.e. oversampling. Similar to the procedure used for oversampling the rows, the column indices are determined via the GappyPOD+E algorithm. While this provides a straightforward approach for *how* to adapt the rank, it does not address *when* the rank should be adapted, or *what* that new rank should be.

Informed by the error analysis from the preceding section, we devise a suitable criterion for controlling the error via rank addition and removal. Since it is not possible to know the true error without solving the expensive FOM, we devise a proxy for estimating the

low-rank approximation error:

$$\epsilon(t) = \frac{\hat{\sigma}_r(t)}{(\sum_{i=1}^r \hat{\sigma}_i(t)^2)^{1/2}}, \quad (26)$$

where $\hat{\sigma}_i$ are the singular values of the low-rank approximation from the previous time step. Assuming the low-rank approximation is near-optimal in its initial condition, we can use the trailing singular value as a proxy for the low-rank approximation error.

To make the error proxy more robust for problems of varying scale and magnitude, we divide by the Frobenius norm of $\hat{\mathbf{V}}$, where it is well-known that $\|\hat{\mathbf{V}}\|_F = (\sum_{i=1}^r \hat{\sigma}_i^2)^{1/2}$. Rather than set a hard threshold, we add/remove modes to maintain ϵ within a desired range, $\epsilon_l \leq \epsilon \leq \epsilon_u$, where ϵ_l and ϵ_u are user-specified lower and upper bounds, respectively. If $\epsilon > \epsilon_u$ we increase the rank to $r + 1$, and if $\epsilon < \epsilon_l$ we decrease the rank to $r - 1$. As a result, this approach avoids the undesirable behavior of repeated mode addition and removal, which is observed by setting a hard threshold. The rank-adaptive TDB-CUR algorithm is detailed in Algorithm 1.

It is important to note that this isn't the only criterion for mode addition and removal, and one can devise a number of strategies based on the problem at hand. However, from our numerical experiments, this approach has proved to be simple and effective, and it does a good job at capturing the trend of the true error. For more details on estimating rank and selection criteria, we refer the reader to [52, Section 2.3]. Finally, it is possible to increase the rank by more than one in Algorithm 1, if required. This can be determined by applying the singular value threshold check after executing Line 19. If $\epsilon > \epsilon_u$ is still true, one more column can be sampled. This requires executing Line 10 to find the new column index, Line 11 to update \mathbf{p} , evaluating \mathbf{V}^k only for the new column using Line 14, and following Lines 15-20. These iterations can be carried out many times, until ϵ falls below ϵ_u .

Remark 1. *Algorithm 1 is presented for solving MDEs that arise from discretizing PDEs with parametric uncertainties, where the rows are dependent on each other but columns can be solved independently. However, Algorithm 1, with minor modification, can be applied to MDEs where the columns are also dependent on each other. In such cases, evaluating $\mathbf{V}^k(:, \mathbf{s})$ requires providing $\hat{\mathbf{V}}^{k-1}(:, [\mathbf{s}, \mathbf{s}_a]) = \mathbf{U}^{k-1} \mathbf{\Sigma}^{k-1} \mathbf{Y}^{k-1}([\mathbf{s}, \mathbf{s}_a], :)^T$, where \mathbf{s}_a is the set of column indices, whose values are needed to compute $\mathbf{V}^k(:, \mathbf{s})$.*

Remark 2. *Algorithm 1 can be applied to problems with dense spatial discretizations, where $\mathbf{p}_a = [1, 2, \dots, n]$. These MDEs can arise, for example, from global discretization methods such as spectral methods. In the most generic form, the computational complexity of computing each entry of the right-hand side matrix \mathbf{F} can be $\mathcal{O}(n^\alpha s^\beta)$ for some $\alpha, \beta \geq 0$. The computational complexity of solving FOM is ns times the computational complexity of each entry, i.e., $\mathcal{O}(ns n^\alpha s^\beta)$ or $\mathcal{O}(n^{(\alpha+1)} s^{(\beta+1)})$. The presented algorithm reduces the cost of evaluating the FOM for this generic setting to $\mathcal{O}((n + s)n^\alpha s^\beta)$.*

For MDEs arising from the discretization of PDEs with parametric uncertainties, $\beta = 0$, and when sparse discretization schemes are used for the spatial discretization, $\alpha = 0$. However, when global discretization methods are used, $\alpha = 1$. Take for example, $\mathcal{F}(t, \mathbf{V}) = \mathbf{D}\mathbf{V}$, where $\mathbf{D} \in \mathbb{R}^{n \times n}$ is a full matrix obtained from discretization of linear differential operators. For this problem, the cost of solving FOM scales with $\mathcal{O}(n^2 s)$, while the cost of solving TDB-CUR scales with $\mathcal{O}(n^2 + ns)$. The toy problem presented in Section 3.1 is a demonstration of a case where there is a dense coupling between both columns and rows.

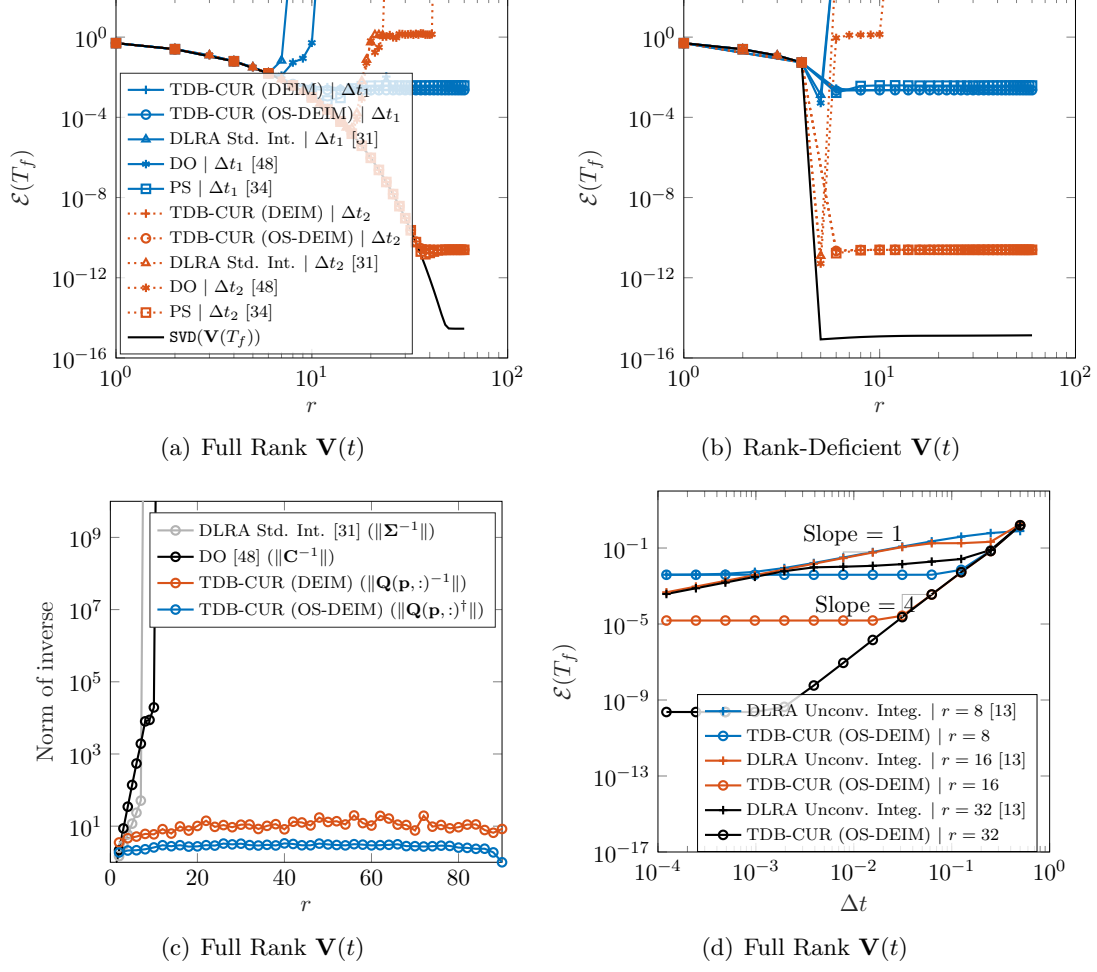


Figure 2: Toy Problem: (a)-(b) Error at the final time $\mathcal{E}(T_f)$ versus reduction order r for step-sizes $\Delta t_1 = 10^{-1}$ and $\Delta t_2 = 10^{-3}$ (c) l^2 norm of the inverse matrix versus reduction order r (d) $\mathcal{E}(T_f)$ versus step size Δt for various reduction orders $r = 8, 16, 32$.

3 Demonstrations

3.1 Toy Problem

As our first example, we compare the accuracy of the presented algorithm against DLRA using standard integrator [31], DO [48], the projector splitting time integrator (PS) [34] and the recently proposed unconventional robust integrator [13]. We emphasize that it is already established that the standard integrator, for example, Runge Kutta schemes, are unstable for solving Eqs. 9a - 9c, which has motivated the development of new time integration techniques [13, 34]. We consider the time-dependent matrix from [13] given explicitly as

$$\mathbf{V}(t) = (e^{t\mathbf{W}_1})e^t\mathbf{D}(e^{t\mathbf{W}_2})^T, \quad 0 \leq t \leq 1.$$

The matrices $\mathbf{W}_1 \in \mathbb{R}^{n \times n}$ and $\mathbf{W}_2 \in \mathbb{R}^{n \times n}$ are randomly generated skew-symmetric matrices as follows: $\mathbf{W}_1 = (\tilde{\mathbf{W}}_1 - \tilde{\mathbf{W}}_1^T)/2$ and $\mathbf{W}_2 = (\tilde{\mathbf{W}}_2 - \tilde{\mathbf{W}}_2^T)/2$, where $\tilde{\mathbf{W}}_1 \in \mathbb{R}^{n \times n}$ and $\tilde{\mathbf{W}}_2 \in \mathbb{R}^{n \times n}$ are uniformly distributed random matrices. The matrix $\mathbf{D} \in \mathbb{R}^{n \times n}$ is diagonal with diagonal entries $d_i = 1/2^i$ for $i \in \{1, 2, \dots, n\}$. We choose $n = 100$ and final time

$T_f = 1$. We create a linear MDE: $d\mathbf{V}/dt = \mathbf{W}_1\mathbf{V} + \mathbf{V} + \mathbf{V}\mathbf{W}_2^T$, where the right-hand side is linearly dependent on \mathbf{V} . We use the explicit fourth-order Runge-Kutta integrator for all of the methods including the substeps of the unconventional robust integrator [13]. We use relative Frobenius error $\mathcal{E}^k = \|\hat{\mathbf{V}}^k - \mathbf{V}^k\|_F / \|\mathbf{V}^k\|_F$ in our analysis.

In Figure 2(a), we plot the error at the final time $\mathcal{E}(T_f)$ versus rank for two different step-sizes: $\Delta t_1 = 10^{-1}$ and $\Delta t_2 = 10^{-3}$. We consider the following cases: TDB-CUR (DEIM), TDB-CUR (OS-DEIM) with $m = 10$, DO [48] (Eqs. 11a-11b), DLRA using standard integrator [31] (Eqs. 9a-9c), and PS [34]. For reference, we also show the optimal error that is obtained via the rank- r SVD of the exact solution at the final time T_f , denoted by $\text{SVD}(\mathbf{V}(T_f))$. For Δt_1 , both DO and DLRA diverge before reaching $r = 10$. This is because the matrix $\mathbf{\Sigma}$ in DLRA and the matrix \mathbf{C} in DO become poorly conditioned as r increases. However, PS, TDB-CUR (OS-DEIM), and TDB-CUR (DEIM) follow the optimal error until the temporal integration error dominates, at which point the error cannot be reduced further by increasing r . It is worth noting that without oversampling, TDB-CUR has a sudden increase in error at around $r = 25$. However, this undesirable behavior is eliminated by oversampling. As the time step is reduced to Δt_2 , we observe a corresponding decrease in the PS, TDB-CUR (DEIM) and TDB-CUR (OS-DEIM) errors. Although DO and DLRA still diverge for the smaller time step, this occurs at a much larger value of r . Thus, Figure 2(a) also highlights the severe time step restrictions for the stability of DO and DLRA in the presence of small singular values.

In Figure 2(b), we consider a rank-deficient matrix and overapproximation using different low-rank techniques. Specifically, we consider the matrix $\mathbf{D} \in \mathbb{R}^{n \times n}$, where the diagonal entries are given by $d_i = 1/2^i$ for $i \in 1, \dots, 5$, and all remaining entries are zero. Our results show that the error drops to the optimal temporal error when $r = 5$. This is because the rank of the matrix is 5. Furthermore, we observe that even in the case of rank deficiency, TDB-CUR remains stable for $r > 5$. This finding supports the observation made in Section 2.5 regarding the conditioning of the presented algorithm. Specifically, even when $r > 5$, the matrix $\mathbf{Q}(\mathbf{p}, :)$ is well-conditioned, and the TDB-CUR scheme remains stable, while both DO and DLRA with standard integrator diverge. Similarly, PS remains stable and converges to the optimal error as it does not require inverting $\mathbf{\Sigma}$.

In Figure 2(c), we plot the l^2 norm of the inverse matrix versus r for all four methods used: $\mathbf{\Sigma}^{-1}$ for DLRA, \mathbf{C}^{-1} for DO, $\mathbf{Q}(\mathbf{p}, :)^{-1}$ for TDB-CUR (DEIM) and $\mathbf{Q}(\mathbf{p}, :)^{\dagger}$ for TDB-CUR (OS-DEIM). As r increases, the matrices $\mathbf{\Sigma}^{-1}$ and \mathbf{C}^{-1} become ill-conditioned, hence the condition numbers for DLRA and DO become unbounded. On the other hand, the condition numbers for TDB-CUR (DEIM) and TDB-CUR (OS-DEIM) remain nearly constant since the matrix $\mathbf{Q}(\mathbf{p}, :)$ is well-conditioned. We also observe that the condition number for TDB-CUR (DEIM) can be improved by oversampling as seen in the plot for TDB-CUR (OS-DEIM).

In the Figure 2(d), we compare $\mathcal{E}(T_f)$ versus step size Δt for various reduction orders $r = 8, 16, 32$. We observe that TDB-CUR (OS-DEIM) saturates to the optimal low-rank error for each r much quicker than using the unconventional robust integrator [13]. Furthermore, the TDB-CUR method retains the fourth-order accuracy of the Runge-Kutta scheme, whereas the order of accuracy for the unconventional robust integrator is first order, despite using fourth-order Runge-Kutta for each substep of the algorithm. This confirms the first-order temporal accuracy of the unconventional integrator [13, Section 3.1].

3.2 Stochastic Burgers Equation

For the second test case, we consider the one-dimensional Burgers equation subject to random initial and boundary conditions as follows:

$$\begin{aligned} \frac{\partial v}{\partial t} + \frac{1}{2} \frac{\partial v^2}{\partial x} &= \nu \frac{\partial^2 v}{\partial x^2}, & x \in [0, 1], t \in [0, 5], \\ v(x, 0; \boldsymbol{\xi}) &= \sin(2\pi x) \left[0.5 \left(e^{\cos(2\pi x)} - 1.5 \right) + \sigma \sum_{i=1}^d \sqrt{\lambda_{x_i}} \psi_i(x) \xi_i \right], & x \in [0, 1], \xi_i \sim \mathcal{N}(\mu, \sigma^2), \\ v(0, t; \boldsymbol{\xi}) &= -\sin(2\pi t) + \sigma \sum_{i=1}^d \lambda_{t_i} \varphi_i(t) \xi_i, & x = 0, \xi_i \sim \mathcal{N}(\mu, \sigma^2), \end{aligned}$$

where $\nu = 2.5 \times 10^{-3}$. The stochastic boundary at $x = 0$ is specified above and the boundary at $x = 1$ is $v(x = 1, t; \boldsymbol{\xi}) = 0$. We use weak treatment of the boundary conditions for both the FOM and TDB [41]. The random space is taken to be $d = 17$ dimensional and ξ_i 's are sampled from a normal distribution with mean $\mu = 0$, standard deviation $\sigma = 0.001$, and $s = 256$. In the stochastic boundary specification, we take $\varphi_i(t) = \sin(i\pi t)$ and $\lambda_{t_i} = i^{-2}$. In the stochastic initial condition, λ_{x_i} and $\psi_i(x)$ are the eigenvalues and eigenvectors of the spatial squared-exponential kernel, respectively. The fourth-order explicit Runge-Kutta method is used for time integration of the FOM and TDB-CUR with $\Delta t = 2.5 \times 10^{-4}$. For discretization of the spatial domain, we use a second-order finite difference scheme on a uniform grid with $n = 401$. This leads to the following MDE of the form $d\mathbf{V}/dt = \mathcal{F}(t, \mathbf{V})$:

$$\frac{d\mathbf{V}(t)}{dt} = -\frac{1}{2} \mathbf{D}_1(\mathbf{V}(t) \odot \mathbf{V}(t)) + \nu \mathbf{D}_2 \mathbf{V}(t) + \mathbf{B}(t), \quad \mathbf{V}(0) = \mathbf{V}_0,$$

where \mathbf{D}_1 and \mathbf{D}_2 are $n \times n$ sparse matrices defining the first and second spatial derivatives of the discretized system. The first and last row of \mathbf{D}_1 and \mathbf{D}_2 are equal to zero. The $n \times s$ matrix $\mathbf{B}(t)$ enforces the stochastic boundary at $x = 0$ by setting each element in its first row equal to $dv(0, t; \boldsymbol{\xi})/dt$, for s independent samples of the random variables $\boldsymbol{\xi}$. All other entries of $\mathbf{B}(t)$ are equal to zero. The columns of \mathbf{V}_0 are the initial conditions for s samples of the random variables.

We first solve the system using TDB-CUR with fixed rank and compare the results against the DLRA and DO by solving Eqs. 9a-9c and Eqs. 11a-11b, respectively. The fourth-order explicit Runge-Kutta method (a standard integrator) is used to solve both the DLRA and DO equations. For TDB-CUR, the rows are oversampled with $m = 5$. No sparse sampling strategy is used for DLRA or DO, and Eqs. 9a-9c and Eqs. 11a-11b are solved as is. In Figure 3(a), we compare the error of TDB-CUR, DLRA, and DO for different values of r . For $r = 6$, TDB-CUR has larger error compared to both DLRA and DO. This result is expected since TDB-CUR has an additional source of error from the sparse sampling procedure. However, as the rank is increased to $r = 9$, the conditioning of the DLRA and DO with standard integrator starts to deteriorate and the error of TDB-CUR is actually lower than DLRA and DO. In fact, for $r > 9$, DLRA and DO with standard integrators are unstable and cannot be integrated beyond the first time step. On the other hand, TDB-CUR remains stable, and the error decays as the rank is increased to a maximum value of $r = 18$. While it is reasonable to expect that the error can be reduced further by increasing the rank to values of $r > 18$, it is important to note that the rank of the initial condition is exactly $r = 18$. Therefore, in order to increase the rank of the system beyond $r = 18$ in

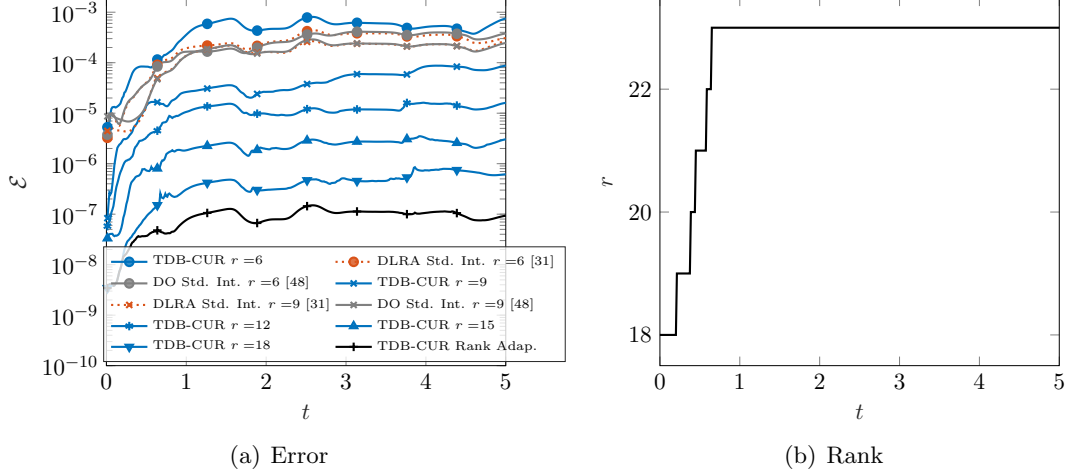


Figure 3: Stochastic Burgers equation with constant diffusion: (a) Relative error evolution for fixed and adaptive rank. (b) Rank evolution using upper threshold $\epsilon_u = 10^{-8}$ for mode addition.

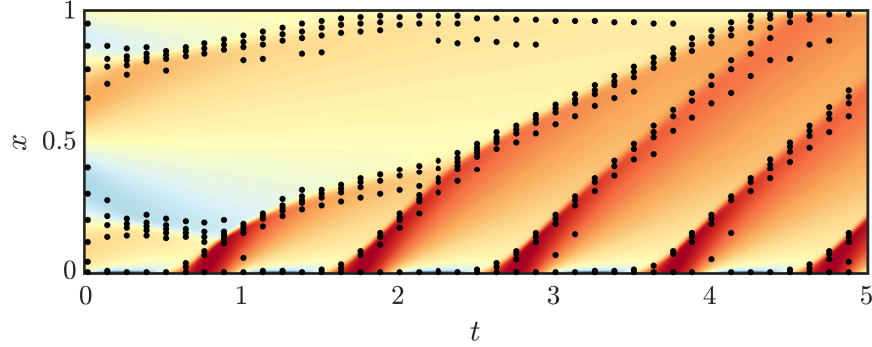


Figure 4: Stochastic Burgers equation with constant diffusion: mean solution with the first 10 QDEIM points (black dots).

a principled manner, we employ the rank adaptive strategy from Section 2.9. To this end, we initialize the system with rank $r_0 = 18$, and use an upper threshold of $\epsilon_u = 10^{-8}$ for mode addition. As observed in Figure 3(b), the rank is increased in time to a maximum of 23, leading to a further reduction in the error.

The mean solution is shown in Figure 4 along with the first 10 QDEIM sampling points. We observe that the sampling points are concentrated near the stochastic boundary at $x = 0$ and also at points in the domain where shocks develop. Figure 5 shows the evolution of the first two spatial modes, \mathbf{u}_1 (top) and \mathbf{u}_2 (bottom), where we observe excellent agreement between the FOM and TDB-CUR. It is important to note that these modes are energetically ranked according to the first and second singular values shown in Figure 6(a). Therefore, we observe that \mathbf{u}_1 captures the large scale energy containing structure, while \mathbf{u}_2 captures the small scale structure that is highly localized in space.

In Figure 6(a), we show that TDB-CUR accurately captures the leading singular values of the FOM solution, despite the large gap between the first and last resolved singular values. Finally, Figure 6(b) compares the CPU time of the FOM, DLRA with the unconventional integrator, and TDB-CUR as the number of rows and columns of the matrix are increased simultaneously. We take $n = s$ and observe that the FOM scales quadratically ($\mathcal{O}(ns)$) while TDB-CUR and DLRA with the unconventional integrator scale linearly ($\mathcal{O}(n + s)$).

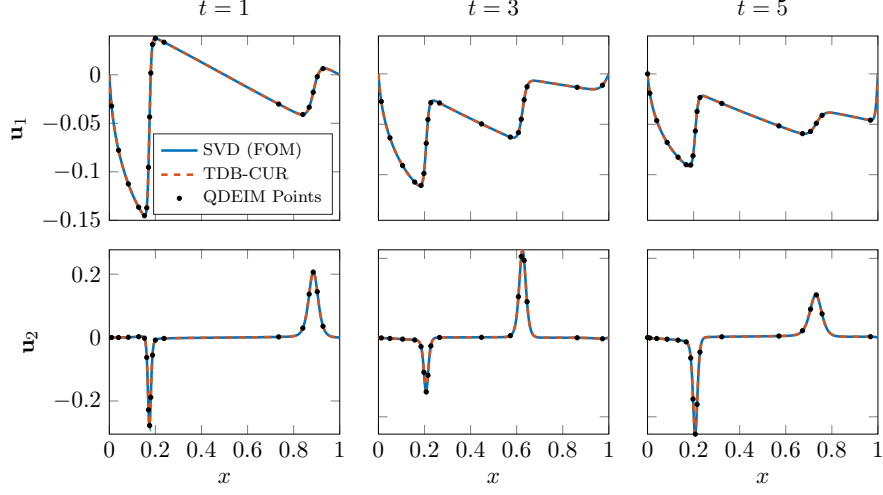


Figure 5: Stochastic Burgers equation with constant diffusion: Evolution of first two spatial modes, \mathbf{u}_1 and \mathbf{u}_2 , and QDEIM points. Excellent agreement between the FOM and TDB-CUR is observed.

As the matrix size is increased, the disparity in CPU time becomes even more apparent, making the case for solving massive MDEs using low-rank approximation. Despite this result, it is important to note that linear scaling for the unconventional integrator is only possible since the nonlinear term in the Burgers equation is limited to quadratic. For higher-order polynomial and general nonlinearities, the unconventional integrator will scale with $\mathcal{O}(ns)$, and exceed the cost of solving the FOM. Nevertheless, given the factored rank- r approximation, $\hat{\mathbf{V}} = \mathbf{U}\mathbf{\Sigma}\mathbf{Y}^T$, the quadratic term can be computed efficiently, resulting in a factorization that has a maximum rank of $(r^2 + r)/2$.

To demonstrate the true power of the TDB-CUR method, we modify the right hand side of the MDE by making the diffusion term nonlinear, $\nu(1 + \tanh(\mathbf{V})\boldsymbol{\xi}') \odot (\mathbf{D}_2\mathbf{V})$. To clarify, \tanh is evaluated element-wise on its argument, and $\boldsymbol{\xi}'$ is an $s \times s$ diagonal matrix with elements drawn from $\mathcal{N}(\mu = 0, \sigma^2 = 0.01^2)$. Furthermore, we verify that $\boldsymbol{\xi}'$ does not result in a negative diffusion. As a result of this simple modification, the cost of directly computing $\mathcal{F}(t, \hat{\mathbf{V}})$ will scale with $\mathcal{O}(ns)$, even for $\hat{\mathbf{V}}$ of low-rank. Therefore, efficient computation of DLRA with a standard integrator [31], unconventional integrator [12], or projection method [30] is not possible. To highlight this, we compare the error versus cost (time to solution) for TDB-CUR, DLRA with the unconventional integrator, and DLRA using projection methods. We use the projected fourth-order Runge-Kutta method (PRK4) presented in [30] along with fourth-order Runge Kutta for both TDB-CUR and the substeps of the unconventional integrator. For the PRK4 method, the unfactored $n \times s$ matrix, \mathbf{F}_i , is computed at the i^{th} stage of the integration scheme. The $n \times s$ matrix is then projected to the tangent space of the rank- r manifold at the i^{th} stage as, $\mathcal{P}_{\mathcal{T}_{\hat{\mathbf{V}}_i}}(\mathbf{F}_i)$, resulting in a matrix whose rank is at most $2r$. Note that using the subscript to denote the stages results in $\hat{\mathbf{V}}_1 = \hat{\mathbf{V}}^{k-1}$. To limit rank growth during the internal steps of the RK4 method, the economy size SVD is applied after each sub-step to obtain the rank- r $\hat{\mathbf{V}}_i = \mathbf{U}_i\mathbf{\Sigma}_i\mathbf{Y}_i^T$. This is only necessary for $i > 1$, since $\hat{\mathbf{V}}_1 = \hat{\mathbf{V}}^{k-1}$ (see above). The orthonormal column and row bases, \mathbf{U}_i and \mathbf{Y}_i , are then used for the tangent space projections at each stage. One final economy size SVD is applied so that the updated low-rank matrix, $\hat{\mathbf{V}}^k$, remains on the rank- r manifold. Although the nonlinear diffusion requires forming \mathbf{F}_i of size $n \times s$, our implementation does not require computing the SVD of matrices larger than $n \times 8r$. To

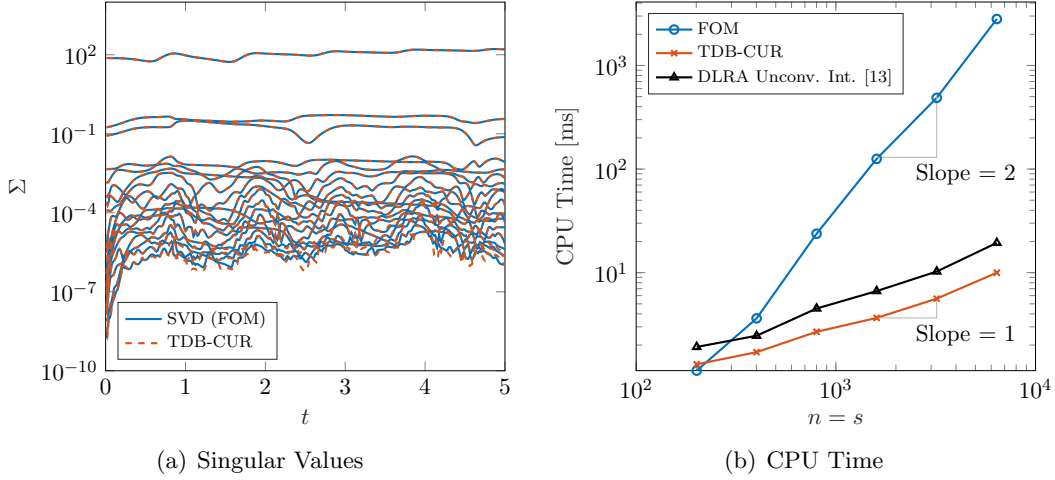


Figure 6: Stochastic Burgers equation with constant diffusion: (a) First 18 singular values of FOM vs TDB-CUR. (b) CPU time for scaling $n = s$ for FOM, TDB-CUR, and the unconventional integrator with fixed $r = 6$.

our knowledge, this represents an efficient implementation of PRK4 when forming the full \mathbf{F}_i cannot be avoided.

Figure 7(a) shows the error versus cost for $r = 6, 9, 12, 15, 18$. For TDB-CUR, we observe a rapid decrease in error for a modest increase in cost. Similar behavior is observed for PRK4, however, both the error and cost exceed those of TDB-CUR. Finally, the unconventional integrator exhibits a larger error than both TDB-CUR and projection for a given Δt . Due to the first-order accuracy of the unconventional integrator, the error does not monotonically decrease as the cost (rank) is increased. To verify this, we decrease Δt by an order of magnitude and rerun. Despite the error dropping by an order of magnitude, the same non-monotonic behavior in the error is observed. This confirms the error in the unconventional integrator is still dominated by the temporal error and not the low-rank approximation error. Finally, we plot the error vs time for TDB-CUR and PRK4 in Figure 7(b). As the rank is increased, we observe a corresponding decrease in the error for both methods. However, TDB-CUR ultimately achieves lower error than PRK4 as the rank is increased.

Although it is not entirely obvious why PRK4 has a larger error as the rank is increased, we propose one possible explanation based on the curvature of the manifold. To this end, it is well known that the curvature of the manifold is inversely proportional to the smallest singular value in the low-rank solution [34, 46]. Therefore, as the rank is increased in the above example, the curvature of the manifold at the low-rank solution increases rapidly. As the curvature increases, the tangent space will no longer provide a good approximation for small deviations (e.g. $\mathcal{O}(\Delta t)$) from the low-rank solution at that point. Since PRK4 takes noninfinitesimal time steps off the rank- r manifold, the subsequent tangent space projections may induce errors that can be large for points on the manifold with high-order curvature. Therefore, one possible explanation for the above result is that the tangent space projection incurs a larger error since its accuracy relies heavily on the curvature of the manifold at that point. On the other hand, the TDB-CUR method does not use tangent space projections, and does not suffer from the high-order curvature of the manifold. For more details, we refer the reader to [15] for an excellent discussion on the error induced by the tangent space projection.

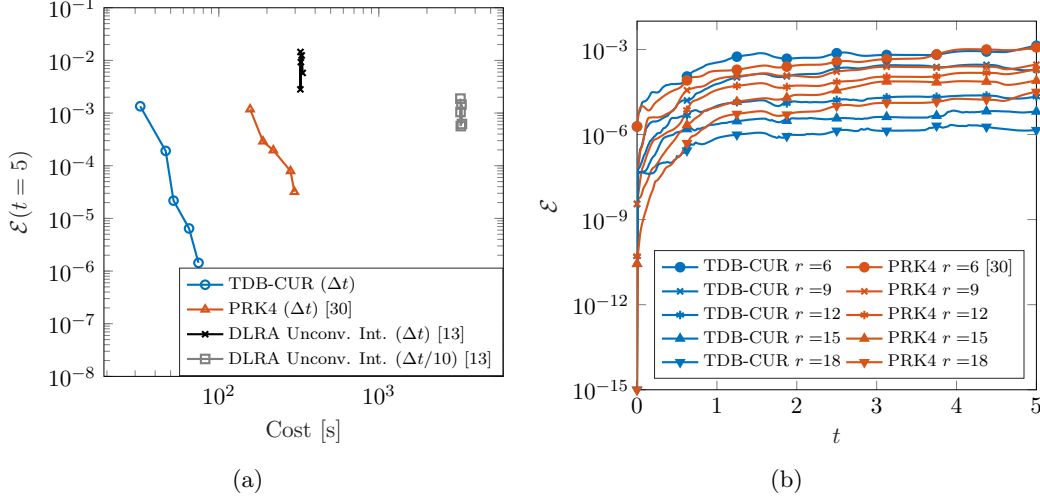


Figure 7: Stochastic Burgers equation with nonlinear diffusion: (a) Error versus time. (b) Error at $t = 5$ versus total cost in seconds. The cost and error data points are obtained by considering $r = 6, 9, 12, 15, 18$.

While Figures 3-7 demonstrate the accuracy, efficiency, rank-adaptivity, and favorable numerical performance of the TDB-CUR method, they do not convey the minimally intrusive nature of its implementation. To give a better perspective on the implementation efforts, the MATLAB code for solving the stochastic Burgers equation using the TDB-CUR method is provided in Appendix A (Listings 1 and 2). While the code contains lines specific to the TDB-CUR method, after reviewing the entire code, it will become apparent that many of the included lines are already required for solving the FOM Burgers equation. Furthermore, there is no term-by-term implementation required to preserve efficiency and the FOM implementation of the Burgers equation (`function f`) is used to compute the sparse row and column samples. Therefore, given an existing FOM implementation, the code required to implement the TDB-CUR method is minimal. The code blocks required for implementing the method are labeled with `%% TDB-CUR` in the attached code.

3.3 Stochastic Advection-Diffusion-Reaction Equation

In this section, we aim to solve the 2D advection-diffusion-reaction (ADR) equation subject to random diffusion coefficient (α), with deterministic initial condition:

$$\begin{aligned} \frac{\partial v}{\partial t} + (u \cdot \nabla)v &= \nabla \cdot (\nabla v \alpha) + \frac{v^2}{10 + v}, \quad x_1 \in [0, 10], x_2 \in [0, 2], t \in [0, 5], \\ v(x_1, x_2, 0) &= \frac{1}{2} \left(\tanh\left(\frac{x_2 + 0.5}{0.1}\right) - \tanh\left(\frac{x_2 - 0.5}{0.1}\right) \right), \end{aligned}$$

where $v(x_1, x_2, t)$ is the species concentration and $u(x_1, x_2, t)$ is the velocity vector. It is worth noting that the nonlinearity of the equation is non-polynomial, implying that the computational expense of DO or DLRA is comparable to that of the FOM. The schematic of the problem is shown in Figure 8. The velocity field is obtained by solving the incompressible Navier-Stokes equations and is independent of the species transport equation. The conditions are identical to those used in previous studies [22, 45]. In particular, we solved the velocity field in the entire domain using the spectral/hp element method on an unstructured mesh with 4008 quadrilateral elements and polynomial order 5. For more

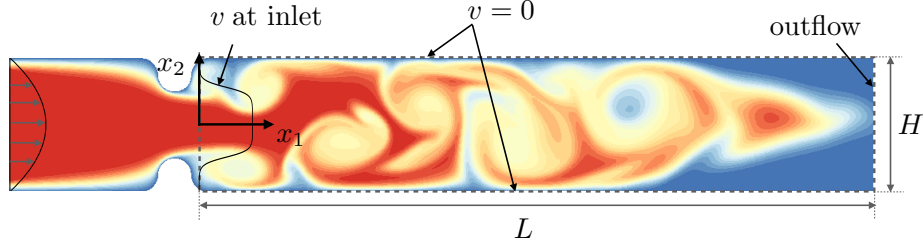


Figure 8: Schematic of the flow visualized with a passive scalar.

details on the spectral element method see for example [5, 29]. At the inlet, a parabolic velocity is prescribed, with an average velocity of \bar{u} . The outflow condition is imposed at the right boundary and the no-slip boundary condition is imposed at the remaining boundaries. The Reynolds number with reference length $H/2$, and kinematic viscosity ν , is given by $Re = \bar{u}H/2\nu = 1000$,

We solved the ADR and TDB-CUR equations using a collocated spectral element method within the rectangular domain indicated by dashed lines in Figure 8. In particular, we use a uniform quadrilateral mesh with 50 elements in the x_1 direction and 15 elements in the x_2 direction, and a spectral polynomial of order 5 in each direction within the rectangular domain. This results in $n = 19076$ degrees of freedom in the spatial domain. We interpolated the velocity field from the unstructured mesh onto the structured mesh. The fourth-order explicit Runge-Kutta method is utilized for time integration with $\Delta t = 5 \times 10^{-4}$ for advancing the ADR and TDB-CUR equations.

Unlike the previous example, we use a deterministic initial condition. Therefore, the rank at $t = 0$ is exactly equal to one, i.e. $\text{rank}(\mathbf{V}(0)) = 1$. While the low-rank approximation with $r = 1$ will be exact in its initial condition, the rank of the system will quickly increase due to the nonlinearity. Therefore, to maintain an acceptable level of error, the rank of the approximation must increase in time. While it is possible to initialize TDB-CUR with $r > 1$, we opt to use the rank-adaptive strategy from Algorithm 1, starting with the initial rank of $r_0 = 1$. Similarly, DLRA using the unconventional integrator can also be initialized with $r > 1$, however, several rank-adaptive integrators have been proposed [14, 20, 55]. On the other hand, initializing DLRA or DO for a standard integrator with $r > 1$ is not possible, as $\mathbf{\Sigma}$ and \mathbf{C} will be singular. Therefore, this problem setup emphasizes the need for rank adaptivity for TDB-based low-rank matrix approximation.

For the first case, we consider a random diffusion coefficient according to $\alpha = \frac{1}{\xi}$, where ξ is a Gaussian random variable with a mean of $\mu = 100$ and standard deviation of $\sigma = 25$. Since validating the performance of TDB-CUR requires solving the FOM, we do not consider a large number of samples for the first case. We draw $s = 50$ samples of the diffusion coefficient, which allows us to compute the error and compare the singular values with the FOM in a reasonable amount of time. Figure 9 shows the evolution of the first three spatial modes, along with the sparse sampling points. As the simulation evolves in time, the points also evolve as the flow is advected from left to right. In Figure 10, the instantaneous singular values from TDB-CUR and the r largest singular values of the FOM solution (SVD singular values) are shown on the left. The discrepancy between the trailing singular values of the TDB-CUR and FOM stems from the effect of unresolved modes in the time integration of the low-rank approximation. However, as observed in the error on the right, accurately resolving the leading singular values results in very small errors. Additionally, the error is controlled by lowering the error threshold for rank addition, leading to improved accuracy

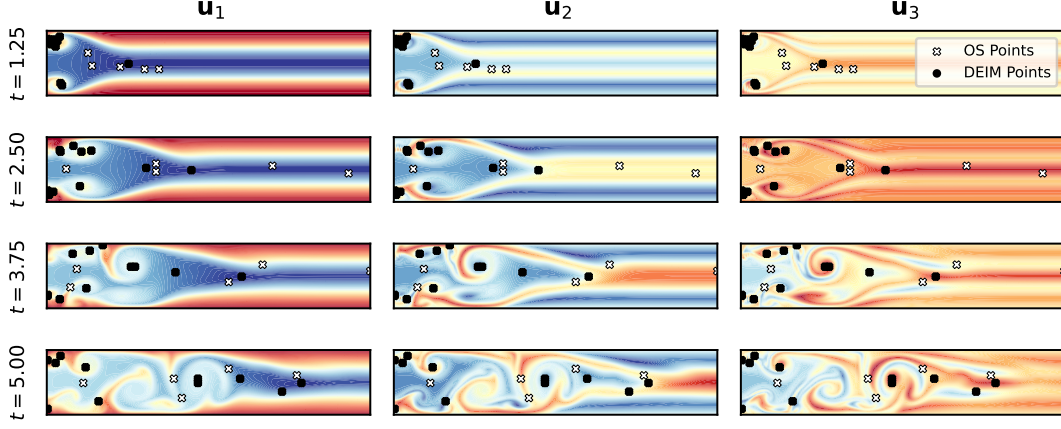


Figure 9: Stochastic Advection-Diffusion-Reaction equation: First three spatial modes of TDB-CUR at different time-steps and the selected points of DEIM with $m = 5$ oversampled (OS) points. ($s = 50$)

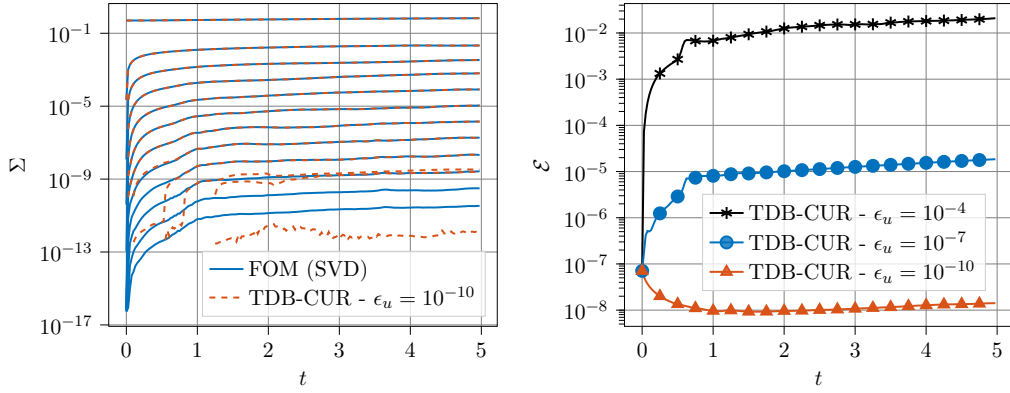


Figure 10: Stochastic Advection-Diffusion-Reaction equation: Left: Comparison of first 10 singular values of FOM vs TDB-CUR with 5 oversampled points ($s = 50$). Right: Error (\mathcal{E}) of TDB-CUR versus time. The result is presented for different values of the upper error bound (ϵ_u) for mode addition.

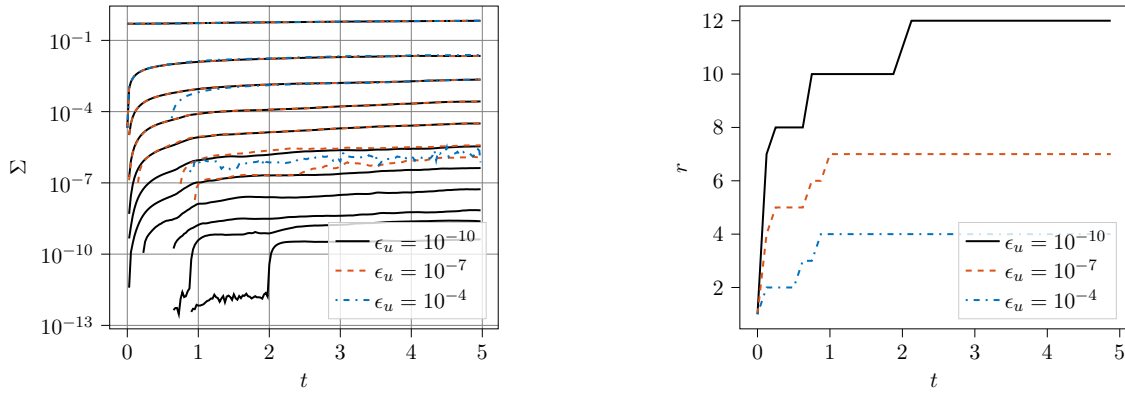


Figure 11: Stochastic Advection-Diffusion-Reaction equation: Left: Singular values of TDB-CUR with 100,000 samples and 5 over-sampled points. Right: Rank versus time. The result is presented for different values of the upper error bound (ϵ_u) for mode addition.

of the TDB-CUR approximation.

In the second case, we take $s = 100,000$ samples of the random diffusion coefficient. This case is of particular interest, as it demonstrates the true potential of the TDB-CUR in cases where the FOM is too costly to run. In order to execute this scenario with the FOM, not only would we require sufficient memory to store the solution matrix of size $n \times s$, we would have to compute the nonlinear map of this massive matrix at each time step. On the other hand, with the new methodology, we never require storing a matrix larger than $n \times r$ or $s \times (m + r)$. To demonstrate this capability, we solve the TDB-CUR with $s = 100,000$ on a laptop computer. Since the available computational resources (our laptop) did not have sufficient memory to store the FOM solution matrix, we could not solve the FOM for comparison. Instead, we performed a convergence study by decreasing the threshold for rank addition, ϵ_u . By decreasing ϵ_u , we observe two things: (i) the rank is increased more rapidly and (ii) the maximum rank is increased. Figure 11 depicts the singular values of the TDB-CUR method versus time (left), and the rank at each time step for different values of ϵ_u (right). As ϵ_u is decreased, the rank is increased, and we observe convergence in the leading singular values.

4 Conclusion

The objective of this work was to develop a method to solve nonlinear matrix differential equations (MDEs) that is accurate, well-conditioned, computationally efficient, and minimally intrusive. To this end, we presented the TDB-CUR algorithm for solving MDEs via low-rank approximation. The algorithm is based on a time-discrete variational principle that leverages sparse sampling to efficiently compute a low-rank matrix approximation at each iteration of the time-stepping scheme. Numerical experiments illustrate that the TDB-CUR algorithm provides a near-optimal low-rank approximation to the solution of MDEs, while significantly reducing the computational cost. Moreover, we showed the method is robust in the presence of small singular values, and significantly outperforms DLRA based on the time continuous variational principle, unconventional integrator, and PRK4. Although not investigated in the present work, the TDB-CUR algorithm is also highly parallelizable, making it an attractive option for high-performance computing tasks.

While the presented approach is minimally intrusive and can be applied to systems containing general nonlinearities, the goal of future work should be to make this method fully non-intrusive, allowing the FOM to be leveraged as a black box. This will allow the method to be applied to proprietary solvers while reducing the overall implementation efforts, making this powerful methodology more accessible to researchers and practitioners, alike.

Acknowledgments

The authors thank Dr. Gianluca Ceruti for numerous insightful and stimulating discussions that led to a number of improvements. This work is supported by the Air Force Office of Scientific Research award FA9550-21-1-0247 and funding from Transformational Tools and Technology (TTT), NASA Grant No. 80NSSC22M0282. Computational resources are provided by the Center for Research Computing (CRC) at the University of Pittsburgh.

A Example Matlab Code

Listing 1: Matlab code to solve the stochastic Burgers equation using TDB-CUR with oversampling

```
close all; clear all; clc
global nu xi d N

rng default
d = 17; sigma = 0.001; % random dimension; standard deviation
Ns = 256; xi = sigma*randn(Ns, d); % # of samples; random parameter samples

dt = 2.5e-4; t0 = 0.0; tf = 5.0; iter_max = round((tf-t0)/dt); save_iter = 50;
nu = 2.5e-3;
N = 401; xmin = 0; xmax = 1; % # of grid points
x = linspace(xmin, xmax, N)'; dx = x(2) - x(1);
e = ones(N,1);
D1 = spdiags([-e, e]/(2*dx), [-1, 1], N, N); D1([1,end], :) = 0; % d/dx
D2 = spdiags([e, -2*e, e]/dx^2, [-1:1], N, N); D2([1,end], :) = 0; % d^2/dx^2

lc = 0.6; K = exp(-(x-x').^2/(2*lc^2)); % squared exponential kernel
[Ux,Lx,~] = svd(K); Ux=Ux(:,1:d); Lx=sqrt(diag(Lx(1:d,1:d)))';
% [Ux,Lx,~] = svds(K,d); Lx=sqrt(diag(Lx));
ub = sin(2*pi*x) .* (0.5*(exp(cos(2*pi*x))-1.5)); % base flow IC
Ux = sin(2*pi*x) .* (Lx.*Ux); % IC perturbations

%% TDB-CUR: initial condition
r = 18; % TDB rank; max=18
m = 5; % # of rows to oversample
U = [ub, Ux];
Y = [ones(Ns,1), xi];
[U, R1] = qr(U, 0);
[Y, R2] = qr(Y, 0);
[RU, S, RY] = svd(R1*R2');
U = U*RU; Y = Y*RY;
U = U(:,1:r); S = S(1:r,1:r); Y = Y(:,1:r);

t = t0;
umean = U*S*sum(Y)'/Ns; tt = 0.0; Sig_TDB = diag(S)';
for iter=1:iter_max % time integration loop
    if mod(iter,100)==0; disp(iter); end

    %% TDB-CUR: compute row and column indices
    s = gpode(Y, r); % column indices
    p = gpode(U, r+m); % rows indices
    [~,pa] = find(D2(p,:)); pa = unique(pa); % adjacent points

    %% TDB-CUR: compute rank-r approximation of G
    u_s = U*S*Y(s,:)' ; u_p = U(p,:) * S*Y'; u_pa = U(pa,:) * S*Y';
    [F1_s, F1_p, F1_pa] = f_ss(t, u_s, u_pa, s, p, pa, D1, D2);
    [F2_s, F2_p, F2_pa] = f_ss(t+0.5*dt, u_s+0.5*dt*F1_s, u_pa+0.5*dt*F1_pa, s, p, pa, D1, D2);
    [F3_s, F3_p, F3_pa] = f_ss(t+0.5*dt, u_s+0.5*dt*F2_s, u_pa+0.5*dt*F2_pa, s, p, pa, D1, D2);
    [F4_s, F4_p, ~] = f_ss(t+dt, u_s+dt*F3_s, u_pa+dt*F3_pa, s, p, pa, D1, D2);
    G_s = u_s + dt*(F1_s+2.0*F2_s+2.0*F3_s+F4_s)/6;
    G_p = u_p + dt*(F1_p+2.0*F2_p+2.0*F3_p+F4_p)/6;
    [U,~] = qr(G_s,0);
    Y = (inv(U(p,:)'*U(p,:))*U(p,:)'*G_p)';
    [Y,S,RU] = svd(Y,0);
    U = U*RU;

    t = iter*dt;
    if mod(iter, save_iter)==0
        tt = [tt t]; umean = [umean, U*S*sum(Y)'/Ns]; Sig_TDB = [Sig_TDB; diag(S)'];
    end
end
subplot(1,2,1), surf(x,tt,umean'), shading interp, view([0 0 1]), hold on; % mean solution (x,t)
subplot(1,2,2), semilogy(tt,Sig_TDB,'LineWidth',2,'Color','k') % singular values vs time

function dudt = f(t, u, D1, D2)
global nu
dudt = -0.5*D1*u.^2 + nu*D2*u; % Burgers equation
end

function out = gdot(t, xi)
global d
out = -2*pi*cos(2*pi*t) + (pi*cos(pi*(1:d).*t)./(1:d))*xi';
end

%% TDB-CUR: compute Burgers rhs (f) at specified rows and columns
function [F_s, F_p, F_pa]=f_ss(t, u_s, u_pa, s, p, pa, D1, D2)
global xi N
F_s = f(t, u_s, D1, D2);
F_s(1,:) = gdot(t,xi(s,:)); F_s(end,:) = 0; % apply boudnary conditions
F_p = f(t, u_pa, D1(p,pa), D2(p,pa));
if ismember(1, p); F_p(1,:) = gdot(t,xi); end % check left boundary (x=0)
if ismember(N, p); F_p(end,:) = 0; end % check right boundary (x=1)
[U_F,~] = qr(F_s,0);
Z_F = inv(U_F(p,:))*U_F(p,:)*U_F(p,:)*F_p;
F_pa = U_F(pa,:)*Z_F;
end
```

Listing 2: GappyPOD+E algorithm adapted from [44]

```

%% TDB-CUR: GappyPOD+E Algorithm
function [ p ] = gpode( U, np )
[~,~,p] = qr(U', 'vector'); % QDEIM (or DEIM)
p = p(1:size(U,2)); % take points equal to number of basis
for i=length(p)+1:np
    [~, S, W] = svd(U(p, :), 0);
    g = S(end-1, end-1)^2 - S(end, end)^2;
    Ub = W'*U';
    r = g + sum(Ub.^2, 1);
    r = r-sqrt((g+sum(Ub.^2,1)).^2-4*g*Ub(end, :).^2);
    [~, I] = sort(r, 'descend');
    e = 1;
    while any(I(e) == p)
        e = e + 1;
    end
    p(end + 1) = I(e);
end
p = sort(p);
end

```

References

- [1] D. Amsallem and C. Farhat. Interpolation method for adapting reduced-order models and application to aeroelasticity. *AIAA Journal*, 46(7):1803–1813, 2023/08/15 2008. doi: 10.2514/1.35374. URL <https://doi.org/10.2514/1.35374>.
- [2] D. Anderson, S. Du, M. Mahoney, C. Melgaard, K. Wu, and M. Gu. Spectral gap error bounds for improving CUR matrix decomposition and the Nyström method. In *Artificial Intelligence and Statistics*, pages 19–27. PMLR, 2015.
- [3] H. Babae. An observation-driven time-dependent basis for a reduced description of transient stochastic systems. *Proceedings of the Royal Society A: Mathematical, Physical and Engineering Sciences*, 475(2231):20190506, 2019. doi: 10.1098/rspa.2019.0506. URL <https://doi.org/10.1098/rspa.2019.0506>.
- [4] H. Babae and T. P. Sapsis. A minimization principle for the description of modes associated with finite-time instabilities. *Proceedings of the Royal Society of London A: Mathematical, Physical and Engineering Sciences*, 472(2186):20150779, 2016. URL <http://dx.doi.org/10.1098/rspa.2015.0779>.
- [5] H. Babae, X. Wan, and S. Acharya. Effect of uncertainty in blowing ratio on film cooling effectiveness. *Journal of Heat Transfer*, 136(3):031701–031701, 11 2013. URL <http://dx.doi.org/10.1115/1.4025562>.
- [6] H. Babae, M. Choi, T. P. Sapsis, and G. E. Karniadakis. A robust bi-orthogonal/dynamically-orthogonal method using the covariance pseudo-inverse with application to stochastic flow problems. *Journal of Computational Physics*, 344: 303–319, 9 2017. doi: <https://doi.org/10.1016/j.jcp.2017.04.057>. URL <http://www.sciencedirect.com/science/article/pii/S0021999117303364>.
- [7] M. Barrault, Y. Maday, N. C. Nguyen, and A. T. Patera. An ‘empirical interpolation’ method: application to efficient reduced-basis discretization of partial differential equations. *Comptes Rendus Mathematique*, 339(9):667–672, 2004. doi: <https://doi.org/10.1016/j.crma.2004.08.006>. URL <https://www.sciencedirect.com/science/article/pii/S1631073X04004248>.

- [8] A. Barth, C. Schwab, and N. Zollinger. Multi-level Monte Carlo finite element method for elliptic PDEs with stochastic coefficients. *Numerische Mathematik*, 119:123–161, 2011.
- [9] M. H. Beck, A. Jäckle, G. A. Worth, and H. D. Meyer. The multiconfiguration time-dependent Hartree (MCTDH) method: a highly efficient algorithm for propagating wavepackets. *Physics Reports*, 324(1):1–105, 1 2000. doi: [http://dx.doi.org/10.1016/S0370-1573\(99\)00047-2](http://dx.doi.org/10.1016/S0370-1573(99)00047-2). URL <http://www.sciencedirect.com/science/article/pii/S0370157399000472>.
- [10] A. Blanchard and T. P. Sapsis. Analytical description of optimally time-dependent modes for reduced-order modeling of transient instabilities. *SIAM Journal on Applied Dynamical Systems*, 18(2):1143–1162, 2019.
- [11] A. Blanchard and T. P. Sapsis. Learning the tangent space of dynamical instabilities from data. *Chaos: An Interdisciplinary Journal of Nonlinear Science*, 29(11), 2019.
- [12] G. Ceruti and C. Lubich. An unconventional robust integrator for dynamical low-rank approximation. *BIT Numerical Mathematics*, 2021. doi: 10.1007/s10543-021-00873-0. URL <https://doi.org/10.1007/s10543-021-00873-0>.
- [13] G. Ceruti and C. Lubich. An unconventional robust integrator for dynamical low-rank approximation. *BIT Numerical Mathematics*, pages 1–22, 2021.
- [14] G. Ceruti, J. Kusch, and C. Lubich. A rank-adaptive robust integrator for dynamical low-rank approximation. *arXiv preprint arXiv:2104.05247*, 2021.
- [15] A. Charous and P. F. Lermusiaux. Dynamically orthogonal runge–kutta schemes with perturbative retractions for the dynamical low-rank approximation. *SIAM Journal on Scientific Computing*, 45(2):A872–A897, 2023.
- [16] S. Chaturantabut and D. C. Sorensen. Nonlinear model reduction via discrete empirical interpolation. *SIAM Journal on Scientific Computing*, 32(5):2737–2764, 2020/12/11 2010. doi: 10.1137/090766498. URL <https://doi.org/10.1137/090766498>.
- [17] S. Chaturantabut and D. C. Sorensen. Nonlinear model reduction via discrete empirical interpolation. *SIAM Journal on Scientific Computing*, 32(5):2737–2764, 2010.
- [18] M. Cheng, T. Y. Hou, and Z. Zhang. A dynamically bi-orthogonal method for time-dependent stochastic partial differential equations i: Derivation and algorithms. *Journal of Computational Physics*, 242(0):843 – 868, 2013. ISSN 0021-9991. doi: <http://dx.doi.org/10.1016/j.jcp.2013.02.033>. URL <http://www.sciencedirect.com/science/article/pii/S0021999113001526>.
- [19] M. Choi, T. P. Sapsis, and G. E. Karniadakis. On the equivalence of dynamically orthogonal and bi-orthogonal methods: Theory and numerical simulations. *Journal of Computational Physics*, 270:1 – 20, 2014. ISSN 0021-9991. doi: <http://dx.doi.org/10.1016/j.jcp.2014.03.050>. URL <http://www.sciencedirect.com/science/article/pii/S002199911400237X>.
- [20] A. Dektor, A. Rodgers, and D. Venturi. Rank-adaptive tensor methods for high-dimensional nonlinear pdes. *Journal of Scientific Computing*, 88(2):1–27, 2021.

- [21] L. Dieci and C. Elia. The singular value decomposition to approximate spectra of dynamical systems. theoretical aspects. *Journal of Differential Equations*, 230(2):502–531, 2006. doi: <http://dx.doi.org/10.1016/j.jde.2006.08.007>. URL <http://www.sciencedirect.com/science/article/pii/S0022039606003263>.
- [22] M. Donello, M. H. Carpenter, and H. Babaee. Computing sensitivities in evolutionary systems: A real-time reduced order modeling strategy. *SIAM Journal on Scientific Computing*, pages A128–A149, 2022/01/19 2022. doi: 10.1137/20M1388565. URL <https://doi.org/10.1137/20M1388565>.
- [23] Z. Drmač and S. Gugercin. A new selection operator for the discrete empirical interpolation method—improved a priori error bound and extensions. *SIAM Journal on Scientific Computing*, 38(2):A631–A648, 2016. doi: 10.1137/15M1019271. URL <https://doi.org/10.1137/15M1019271>.
- [24] L. Einkemmer and C. Lubich. A low-rank projector-splitting integrator for the vlasov–poisson equation. *SIAM Journal on Scientific Computing*, 40(5):B1330–B1360, 2023/08/15 2018. doi: 10.1137/18M116383X. URL <https://doi.org/10.1137/18M116383X>.
- [25] C. Farhat, P. Avery, T. Chapman, and J. Cortial. Dimensional reduction of nonlinear finite element dynamic models with finite rotations and energy-based mesh sampling and weighting for computational efficiency. *International Journal for Numerical Methods in Engineering*, 98(9):625–662, 2023/08/15 2014. doi: <https://doi.org/10.1002/nme.4668>. URL <https://doi.org/10.1002/nme.4668>.
- [26] M. B. Giles. Multilevel Monte Carlo path simulation. *Operations research*, 56(3):607–617, 2008.
- [27] N. Halko, P.-G. Martinsson, and J. A. Tropp. Finding structure with randomness: Probabilistic algorithms for constructing approximate matrix decompositions. *SIAM review*, 53(2):217–288, 2011.
- [28] J. Hu and Y. Wang. An adaptive dynamical low rank method for the nonlinear boltzmann equation. *Journal of Scientific Computing*, 92(2):75, 2022. doi: 10.1007/s10915-022-01934-4. URL <https://doi.org/10.1007/s10915-022-01934-4>.
- [29] G. E. Karniadakis and S. J. Sherwin. *Spectral/hp element methods for computational fluid dynamics*. Oxford University Press, USA, 2005.
- [30] E. Kieri and B. Vandereycken. Projection methods for dynamical low-rank approximation of high-dimensional problems. *Computational Methods in Applied Mathematics*, 19(1):73–92, 2019.
- [31] O. Koch and C. Lubich. Dynamical low-rank approximation. *SIAM Journal on Matrix Analysis and Applications*, 29(2):434–454, 2017/04/02 2007. doi: 10.1137/050639703. URL <http://dx.doi.org/10.1137/050639703>.
- [32] F. Y. Kuo, C. Schwab, and I. H. Sloan. Quasi-Monte Carlo finite element methods for a class of elliptic partial differential equations with random coefficients. *SIAM Journal on Numerical Analysis*, 50(6):3351–3374, 2012.

- [33] Kusch, J. and Stammer, P. A robust collision source method for rank adaptive dynamical low-rank approximation in radiation therapy. *ESAIM: M2AN*, 57(2):865–891, 2023. doi: 10.1051/m2an/2022090. URL <https://doi.org/10.1051/m2an/2022090>.
- [34] C. Lubich and I. V. Oseledets. A projector-splitting integrator for dynamical low-rank approximation. *BIT Numerical Mathematics*, 54(1):171–188, 2014. doi: 10.1007/s10543-013-0454-0. URL <http://dx.doi.org/10.1007/s10543-013-0454-0>.
- [35] M. W. Mahoney and P. Drineas. CUR matrix decompositions for improved data analysis. *Proceedings of the National Academy of Sciences*, 106(3):697–702, 2009.
- [36] K. Manohar, B. W. Brunton, J. N. Kutz, and S. L. Brunton. Data-driven sparse sensor placement for reconstruction: Demonstrating the benefits of exploiting known patterns. *IEEE Control Systems Magazine*, 38(3):63–86, 2018. doi: 10.1109/MCS.2018.2810460.
- [37] E. Musharbash and F. Nobile. Dual dynamically orthogonal approximation of incompressible Navier [Stokes equations with random boundary conditions. *Journal of Computational Physics*, 354:135–162, 2018. doi: <https://doi.org/10.1016/j.jcp.2017.09.061>. URL <http://www.sciencedirect.com/science/article/pii/S0021999117307349>.
- [38] M. H. Naderi and H. Babaei. Adaptive sparse interpolation for accelerating nonlinear stochastic reduced-order modeling with time-dependent bases. *Computer Methods in Applied Mechanics and Engineering*, 405:115813, 2023. doi: <https://doi.org/10.1016/j.cma.2022.115813>. URL <https://www.sciencedirect.com/science/article/pii/S0045782522007691>.
- [39] A. G. Nouri, H. Babaei, P. Givi, H. K. Chelliah, and D. Livescu. Skeletal model reduction with forced optimally time dependent modes. *Combustion and Flame*, page 111684, 2021. doi: <https://doi.org/10.1016/j.combustflame.2021.111684>. URL <https://www.sciencedirect.com/science/article/pii/S0010218021004272>.
- [40] P. Patil and H. Babaei. Real-time reduced-order modeling of stochastic partial differential equations via time-dependent subspaces. *Journal of Computational Physics*, 415:109511, 2020. doi: <https://doi.org/10.1016/j.jcp.2020.109511>. URL <http://www.sciencedirect.com/science/article/pii/S0021999120302850>.
- [41] P. Patil and H. Babaei. Reduced-order modeling with time-dependent bases for pdes with stochastic boundary conditions. *SIAM/ASA Journal on Uncertainty Quantification*, 11(3):727–756, 2023.
- [42] B. Peherstorfer. Model reduction for transport-dominated problems via online adaptive bases and adaptive sampling. *SIAM Journal on Scientific Computing*, 42(5):A2803–A2836, 2020. doi: 10.1137/19M1257275. URL <https://doi.org/10.1137/19M1257275>.
- [43] B. Peherstorfer and K. Willcox. Online adaptive model reduction for nonlinear systems via low-rank updates. *SIAM Journal on Scientific Computing*, 37(4):A2123–A2150, 2015. doi: 10.1137/140989169. URL <https://doi.org/10.1137/140989169>.
- [44] B. Peherstorfer, Z. Drmac, and S. Gugercin. Stability of discrete empirical interpolation and gappy proper orthogonal decomposition with randomized and deterministic sampling points. *SIAM Journal on Scientific Computing*, 42(5):A2837–A2864, 2020.

- [45] D. Ramezani, A. G. Nouri, and H. Babaee. On-the-fly reduced order modeling of passive and reactive species via time-dependent manifolds. *Computer Methods in Applied Mechanics and Engineering*, 382:113882, 2021. doi: <https://doi.org/10.1016/j.cma.2021.113882>. URL <https://www.sciencedirect.com/science/article/pii/S004578252100219X>.
- [46] A. Rodgers, A. Dektor, and D. Venturi. Adaptive integration of nonlinear evolution equations on tensor manifolds. *Journal of Scientific Computing*, 92(2):39, 2022.
- [47] D. Ryckelynck. A priori hyperreduction method: an adaptive approach. *Journal of Computational Physics*, 202(1):346–366, 2005. doi: <https://doi.org/10.1016/j.jcp.2004.07.015>. URL <https://www.sciencedirect.com/science/article/pii/S002199910400289X>.
- [48] T. Sapsis and P. Lermusiaux. Dynamically orthogonal field equations for continuous stochastic dynamical systems. *Physica D: Nonlinear Phenomena*, 238(23-24):2347–2360, 2009.
- [49] S. Schotthöfer, E. Zangrando, J. Kusch, G. Ceruti, and F. Tudisco. Low-rank lottery tickets: finding efficient low-rank neural networks via matrix differential equations, 2022.
- [50] D. C. Sorensen and M. Embree. A DEIM induced CUR factorization. *SIAM Journal on Scientific Computing*, 38(3):A1454–A1482, 2016.
- [51] D. B. Szyld. The many proofs of an identity on the norm of oblique projections. *Numerical Algorithms*, 42(3):309–323, 2006. doi: [10.1007/s11075-006-9046-2](https://doi.org/10.1007/s11075-006-9046-2). URL <https://doi.org/10.1007/s11075-006-9046-2>.
- [52] R. Vidal, Y. Ma, and S. Sastry. Generalized principal component analysis (GPCA). *IEEE transactions on pattern analysis and machine intelligence*, 27(12):1945–1959, 2005.
- [53] K. Wright. Differential equations for the analytic singular value decomposition of a matrix. *Numerische Mathematik*, 63(1):283–295, 1992. doi: [10.1007/BF01385862](https://doi.org/10.1007/BF01385862). URL <http://dx.doi.org/10.1007/BF01385862>.
- [54] D. Xiu and J. Hesthaven. High-order collocation methods for differential equations with random inputs. *SIAM Journal on Scientific Computing*, 27(3):1118, 2006.
- [55] M. Yang and S. R. White. Time-dependent variational principle with ancillary krylov subspace. *Physical Review B*, 102(9):094315, 2020.
- [56] R. Zimmermann and K. Willcox. An accelerated greedy missing point estimation procedure. *SIAM Journal on Scientific Computing*, 38(5):A2827–A2850, 2023/08/15 2016. doi: [10.1137/15M1042899](https://doi.org/10.1137/15M1042899). URL <https://doi.org/10.1137/15M1042899>.